Negative ion formation in the scattering of atoms and ions from dielectric surfaces

2000 J. Phys.: Condens. Matter 12 R177

(http://iopscience.iop.org/0953-8984/12/13/201)

J. Phys.: Condens. Matter **12** (2000) R177–R206. Printed in the UK PII: S0953-8984(00)10152-3

REVIEW ARTICLE

Negative ion formation in the scattering of atoms and ions from dielectric surfaces

A G Borisov and V A Esaulov

Laboratoire des Collisions Atomiques et Moléculaires (Unité de Recherche mixte CNRS–Université Paris-Sud, UMR8625), bâtiment 351, Université de Paris-Sud, 91415 Orsay Cédex, France

Received 6 November 1999

Abstract. Interaction of atomic and molecular particles with dielectric surfaces has been attracting considerable attention over the past years, in order to understand various fundamental problems important in catalysis, development of gas sensors, problems of adhesion etc. Detailed quantitative information about the dynamics of electron transfer, which plays an important role in chemisorption and reactions at surfaces, has been recently obtained from experiments in which ionic or atomic beams are scattered off dielectric surfaces and the charge states of particles are analysed, providing in particular site-specific information on electron transfer. These experiments have shown that the dynamics of electron transfer on semiconductor and insulator surfaces cannot be understood within simple models extensively used for the case of metal surfaces. It was shown in particular that in spite of the existence of large bandgaps and at first sight the unfavourable situation for resonant electron transfer, negative ion formation occurs quite efficiently. Together with the existence of an efficient electron capture process associated with negative ion formation the existence of electron loss processes was demonstrated by use of both atoms and negative ions as projectiles. Various theoretical descriptions for describing electron capture and loss phenomena have been developed. In this review the experimental approaches and results are outlined along with the theoretical concepts and approaches developed to treat electron transfer phenomena on dielectric surfaces.

1. Introduction

This review deals with the electron transfer process in the interaction of atoms with dielectric surfaces. Dielectric surfaces are of considerable technological and heuristic interest (Somorjai 1981, King and Woodruf 1988, Henrich and Cox 1994, Noguera 1996). Numerous experimental and theoretical studies have been performed for the case of semiconductors and an increasing amount of surface science work is now being devoted to the study of insulating surfaces, such as oxides, alkali halides etc (see e.g. Colbourn 1992, Freund and Umbach 1993, Henrich and Cox 1994, Noguera 1996, Freund 1997). Much of this work is done with the aim of understanding fundamental problems in catalysis, gas sensors, adhesion etc. A variety of surface processes such as chemisorption and reactions on surfaces frequently involve an electron transfer step as has for instance been discussed for the example of H^+ and OH^- adsorption on a series of oxides (Goniakowski *et al* 1993). Detailed quantitative information about the dynamics of the electron transfer at surfaces can be obtained from experiments in which ionic or atomic beams are scattered off the surface and the charge states of particles are analysed. Since the energy and specific scattering trajectory can be selected, these experiments allow one to obtain information in controlled temporal conditions. Moreover, the *site-specific information* can be extracted. A number of such scattering experiments have been performed

0953-8984/00/130177+30$30.00

in the past for the case of metals and have provided data allowing rigorous tests of theoretical predictions about the modifications of atomic or molecular states in front of surfaces (Brako and Newns 1989, Los and Geerlings 1990, Winter 1991, Burgdörfer 1993, Heiland and Närmann 1993, Rabalais 1994, Behringer *et al* 1996). For the very important case of semiconductor and insulator surfaces, such studies are still fairly scarce, though in the past few years some exciting new data have been obtained on ion yields in scattering from dielectrics (e.g. Guseva *et al* 1991, Souda *et al* 1995, Auth *et al* 1995a, Maazouz *et al* 1996c, 1998, Ustaze *et al* 1997a, b, c, Meyer *et al* 1997, Wurtz *et al* 1997), resonant coherent excitation of scattered atoms (Kimura *et al* 1996, Kimura and Mannamie 1998, Auth *et al* 1997), energy thresholds for the projectile stopping and discrete structures in the energy loss spectra (Souda *et al* 1993a, b, 1998, Auth *et al* 1998a, Roncin *et al* 1999) as well as on sputtering of the ionic crystals (Fine 1993, Hayderer *et al* 1999).

In this review we shall discuss the case of negative ion formation in the *scattered beams*. Detailed discussions on *sputtering* of negative ions from dielectric surfaces by ion beam bombardment can be found in e.g. Yu (1991), Varga and Diebold (1994) and Kasi *et al* (1989).

Since our present understanding of the projectile charge state evolution in surface scattering events stems mainly from projectile/metal surface interaction studies, it would be useful to recall here the main features of negative ion formation in this case. At metal surfaces negative ion formation/destruction proceeds via one-electron energy-conserving transitions between the electronic states of the valence band of the metal and affinity level of the projectile. This is the so-called resonant charge transfer (RCT) process. Details on the RCT process can be found in a number of review papers (see e.g. Brako and Newns 1989, Los and Geerlings 1990, Rabalais 1994). Briefly, when an atomic projectile approaches a metal surface its affinity level broadens into the resonance because of the coupling with continuum of electronic states of the metal. Furthermore, it experiences a downward shift due to the image potential as schematized in figure 1(a). The width Γ of the affinity level gives the rate of the projectile–surface electron transfer. Usually Γ decreases exponentially with increasing projectile–surface distance. The energy shift of the affinity level (δE) is given by $\delta E = -1/4Z$, where Z is the ion–surface distance along the surface normal measured from the image plane. Even though in most of the cases binding energies of negative ions are smaller than typical work function values of metal surfaces, owing to this image shift the anion level might cross the Fermi level of the surface at a certain distance Z_F. Consider the case of an atom, which moves away from the surface. The population of the anion level can occur at small projectile surface separations ($Z < Z_F$) by resonant electron capture from the occupied valence band states below the Fermi level. For larger distances ($Z > Z_F$) resonant loss to the unoccupied valence band states above the Fermi level will deplete the population of the anion level. The final negative ion fraction will depend on the electron transfer rates Γ and the time spent in the two regions.

The situation is slightly more complicated in the case of the fast small-angle (grazing) scattering from the surface. The electronic states of the metal and those of the projectile are defined in the reference frames moving one with respect to the other which leads to the so-called 'parallel velocity' effect. Usually, it is discussed in terms of the free electron picture of the shifted Fermi sphere model, which takes into account the fact that the energy distribution of the metal electrons is modified as seen from the moving projectile frame (Doppler–Fermi–Dirac distribution) (van Wunnik *et al* 1983, Brako and Newns 1989, Los and Geerlings 1990, Winter 1991). This leads to a characteristic dependence of the negative ion yield on the velocity of the scattered beam parallel to the surface (Los and Geerlings 1990, Winter 1991, Folkerts *et al* 1995, Maazouz *et al* 1996a, b, Auth *et al* 1998c, Lorente *et al* 1999).

The electronic structure of semiconductors is distinguished by e.g. the existence of a bandgap and surface states (Qian and Chadi 1987, Ciraci *et al* 1984, Biswas *et al* 1989) that

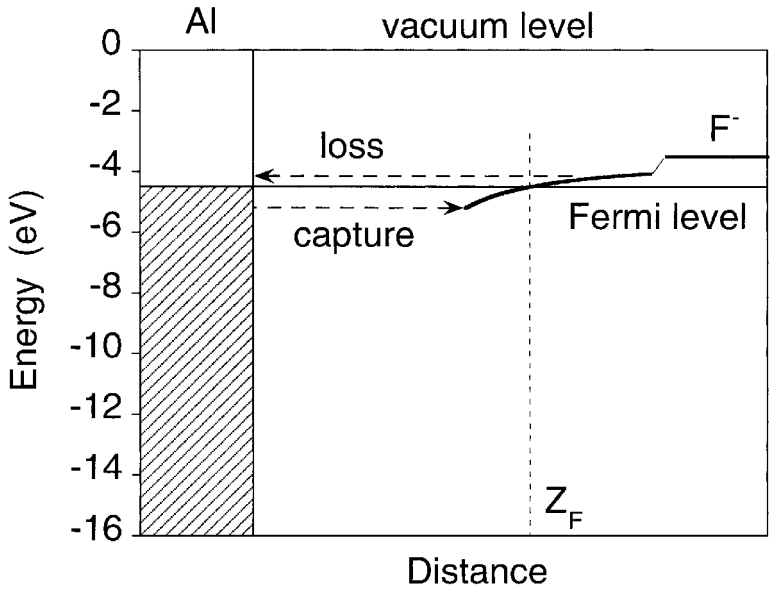

(a)

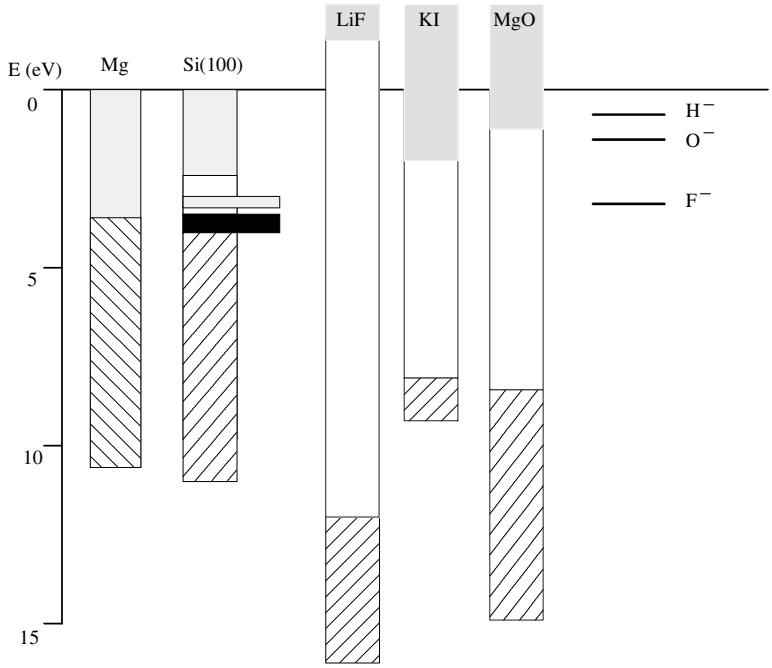

(b)

Figure 1. (a) Energy-level diagram for an F^- ion in front of a metal (Al) surface. The hatched area indicates occupied states in the valence band. (b) Schematic diagram of the H^-, O^- and F^- affinity levels relevant for the electron capture process on Mg, Si(100), LiF, KI and MgO (Tjeng *et al* 1990). The electron affinities of H^-, O^- and F^- are 0.754 eV, 1.462 eV and 3.399 eV respectively (see e.g. Esaulov 1986). Note that while the bulk gap for MgO is 7.5 eV (as shown), the surface gap is about 6.5 eV. The position of the conduction band is indicated for ionic crystals by the grey area.

play an important role in their surface chemistry. As an example the Si(100) structure is schematized in figure 1(b). Here the bandgap is about 1.1 eV and the occupied states lie about 5 eV below the vacuum level (Ciraci *et al* 1984). In this case on the one hand, resonant capture could be less efficient than on e.g. the Al surface (work function ∼4.3 eV) since the anion level shift required to bring it into resonance with occupied states has to be higher implying shorter atom–surface distances. On the other hand the existence of a gap could hinder loss processes. Furthermore, the free-electron-like treatment of the parallel velocity effects should be inappropriate in this case. The situation thus looks quite different from the case of the scattering from the metal surfaces and one might expect some differences in negative ion formation rates.

The case of wide bandgap ionic-crystal insulators like some oxides or alkali halides is again very different from the free electron metal case. The affinity levels of gas phase negative ions usually lie in the bandgap of ionic solids as schematized in figure 1(b). The shift of the affinity level of the projectile in front of the dielectric surface in the static case (no projectile motion) is given by $\delta E = -[\varepsilon(0) - 1]/[\varepsilon(0) + 1]/4Z$ where $\varepsilon(0)$ is a static dielectric constant. The dynamical situation is quite different. Indeed, the dielectric constant depends on the characteristic time scale (frequency ω) of the external field ($\varepsilon = \varepsilon(\omega)$). For example, for the LiF crystal $\varepsilon(0)$ is equal to 9 while the 'optical value' is $\varepsilon(\infty) = 1.92$ (Lowndes and Martin 1969). The frequency dependent dielectric constant $\varepsilon(\omega)$ can be used to calculate the dynamical response of the surface on the field of the moving projectile (Garcia de Abajo and Echenique 1992). In case of ionic crystals it was demonstrated (Auth *et al* 1995b, Hägg *et al* 1997, Ducrée *et al* 1998) that owing to relatively large velocities of the scattered projectiles ions of the crystal lattice do not have enough time to respond to the field of the moving charge. Therefore the 'effective' dielectric constant is given mainly by the electronic response and $\delta E = -[\varepsilon(\infty) - 1]/[\varepsilon(\infty) + 1]/4Z$. For the same distance Z the affinity level shift δE is much reduced compared to the case of the metal surface. An estimate of the image potential effect for a moving charge in ion scattering on LiF gave a value of 1 to 2 eV (Auth *et al* 1995a, b) for grazing scattering conditions. Thus one would expect that the image potential effect is not able to provide the significant downward shift of the affinity level required to bring it into resonance with the occupied states of the valence band. On the basis of this picture one could conclude that negative ion formation would not occur. However, as we shall see below, it does occur most efficiently and this can be understood in rather simple terms.

In the following, after a brief discussion of the types of experiment that have been performed and some experimental problems in section 2, we shall summarize the main experimental findings. Negative ion formation on covalent dielectric (Si, GaAs, and diamond) surfaces is discussed in section 3. Results for the negative ion formation on ionic solids (oxides and halides) are then presented (section 4) along with the theoretical descriptions that have been proposed (section 5).

2. Experimental aspects

Most experiments performed used fairly standard approaches except for one of the latest measurements involving an electron–atom/ion *coincidence* technique. Here we shall briefly mention the types of measurement made and point out some specific characteristics of experiments dealing with insulators, residing in problems associated with charging and surface preparation. In most cases experiments usually involved

(a) ion fraction measurements (see e.g. Shi *et al* 1989, Auth *et al* 1995a, 1998b, Meyer *et al* 1997, Maazouz *et al* 1996a, b, c, Ustaze *et al* 1997a, b, c) for some given scattering configurations with regard to incident and reflected angles,

(b) ion scattering spectroscopy or energy loss measurements (see e.g. Souda *et al* 1992, 1993a, b, 1995, 1998, 1999a, b, Souda and Yamamoto 1997, Souda 1997, Auth *et al* 1998a, Casagrande *et al* 2000, Roncin *et al* 1999) of backscattered positive and negative ions and

(c) in some cases electron spectroscopy of slow electrons resulting from slow ion–surface interactions was performed (Stracke *et al* 1997, Kempter 1998).

The charge fraction measurements give quantitative information about the probability of electron capture for the given scattering conditions and hence for a given velocity component of the atom perpendicular and parallel to the surface. The ion fractions are usually defined as the ratio of the particle flux in a given charge state to the total flux (for a given detection angle with respect to the surface plane). The energy loss measurements (ISS) allow one to determine the site at which electron capture occurs (e.g. cation or anion in an ionic solid). These measurements have also revealed the existence of discrete energy losses in large angle scattering (Souda *et al* 1993a, b, 1995) and more recently for grazingly scattered beams (Auth *et al* 1998a, Roncin *et al* 1999). Detailed information on the projectile surface interaction was obtained in coincidence experiments using a novel type of multicoincidence detector (Roncin *et al* 1999) allowing the monitoring of energy losses in ion/atom scattering in coincidence with electron emission, where electrons emitted into a 2π sterad solid angle above the surface were collected. An electron spectroscopy study (Stracke *et al* 1997, Kempter 1998) provided interesting information on short lived states produced as a result of electron transfer.

The main specific characteristic of studies involving positively or negatively charged particle beams is that they generally lead to positive (or negative) charging up of the insulator. For good insulators this charging up will finally result in a complete reflection of the beam away from the surface. For intermediate charging the scattered ion can still be shifted in energy. Not only primary but also secondary ion production can be affected. A common practice both for positive ion scattering and also for the case of negatively charged particles (electrons or negative ions) is to spray the surface with an electron beam. Both low energy (a few eV) and high energy (keV) electron beams have been used in ion scattering experiments (see e.g. Brongersma *et al* 1994) and in HREELS (Coustet and Jupille 1994) on oxides. It has been suggested by Brongersma *et al* that in the case of a rough surface like that of an oxide catalyst the direction of the incident ion beam and neutralizing electron beam should coincide so that the proper part of the surface is neutralized. Note that in certain cases the use of high energy electrons could lead to defect formation. This is especially the case of the alkali halide crystals where electron stimulated desorption is extremely efficient (Szymonski 1990). An alternative method relies on increasing the electrical conductivity of the target. This can be achieved by heating the sample as has been used for zeolites (Grünert *et al* 1993) and for alkali halides (see e.g. Varga and Diebold 1994, Auth *et al* 1995a, b). Another possibility consists in using, instead of bulk dielectrics, dielectric films deposited on a metallic support (Dieckhoff *et al* 1992, Cornille *et al* 1994, Chen and Goodman 1994, Wiegershaus *et al* 1996, Stracke *et al* 1997).

Besides the problem of charging an important aspect for grazing scattering experiments is the problem of generating clean, flat and defect free surfaces. Large flat area (several thousand atomic units) samples of MgO(001) can be prepared by cleaving in vacuum. An alternative method used for grazing x-ray diffraction consists in bakeouts in air followed, in vacuum, by sputtering at high temperatures and annealing in the presence of oxygen in order to reduce oxygen vacancies (see e.g. Renaud *et al* 1994). Removal of contaminants such as adsorbed water and hydrocarbons can be achieved by heating the target. Use of sputtering can result in some cases in severe alterations of surface stoichiometry. A clear manifestation of this is the appearance of structure in the gap region in EELS studies (see e.g. Henrich and Cox

1994). In the case of alkali halides clean and flat (001) surfaces were obtained by Auth *et al* (1995a, b, 1998b) and Winter *et al* (1996a) by large number of cycles of *grazing* sputtering (to reduce erosion phenomena) with 20 keV Ar^+ ions (incidence angle 1.6° from the surface plane) at 330 °C and subsequent annealing for some minutes at about 400 °C. At 400 °C radiation induced lattice defects are annealed and a stoichiometric surface is restored (see Varga and Diebold 1994, Wurz and Becker 1989). In order to reduce directional effects the target was azimuthally rotated in intervals of about 1.5° with a sputtering time of 1–2 s per position.

3. Negative ion formation on covalent dielectrics

Electron transfer in scattering of atomic/molecular projectiles from the surfaces of covalent dielectrics has not been investigated in much detail except for the isolated cases of Si (Verbeek *et al* 1980, O'Connor and MacDonald 1980, Rechtein *et al* 1990, Kurnaev *et al* 1993, Hird *et al* 1993, Maazouz *et al* 1997, 1998), GaAs (Morris *et al* 1995, 1997, Martin *et al* 1994, 1996) and diamond (Wurtz *et al* 1997, Scheer *et al* 1999).

Results of H^- and O^- ion fraction measurements reported by Maazouz *et al* (1997, 1998) are shown in figure 2. The ion fraction is defined as the ratio of the negative ion flux to the total flux scattered into a given angle. The surprising feature of these data is that the ion fractions are of the same order of magnitude as for an aluminium target (Maazouz *et al* 1996a, b, 1997). Thus the O^- ion fractions on Al (Maazouz *et al* 1997) and Si surfaces at a 4 keV incident energy, have a quantitatively similar dependence on the exit angle to the surface (figure 2). For small angles, i.e. small velocities or long dwelling times of the particle near the surface the negative ion yield was small and increased for shorter dwelling times or large scattering angles. The evolution with ion energy was also found to be similar. Maazouz *et al* (1997, 1998) also investigated the question of dynamic 'parallel velocity' effects that are important for metals. It was found that as in the case of Al for small angle scattering the ion fractions measured for a given perpendicular velocity increased with increasing parallel velocity. This is illustrated in figure 2(b), where data for H^- formation on Si and Al are compared. Thus, in spite of the differences in electronic structure between Si (semiconductor) and Al (free-electron-like metal) there was no significant difference in negative ion formation.

Another example where rather interesting results were obtained is the case of diamond, a covalent insulator with a ∼5.5 eV bandgap. Wurz *et al* (1997) found very large ion fractions of H^- and O^-. Thus ion fractions of the order of 5 to 10% were reported for H^- and of about 30% for O^-. It should be noted however that the surface (polycrystalline diamond deposited on Si) cleanliness in this experiment is difficult to evaluate.

Let us now consider the general characteristics of the negative ion fractions. For the case of metal targets (see e.g. Maazouz *et al* 1996a, b), the increase of the negative ion yield with exit angle can be qualitatively related to a larger survival of negative ions for higher perpendicular velocities $v_\perp$ with respect to the surface plane, or in other words for shorter dwelling times near the surface. Indeed, the negative ion survival probability is proportional to $\exp(-\Gamma v_\perp)$ for the free-electron-like metal surface (Los and Geerlings 1990). A similar interpretation of the exit angle dependence could be given here. However in practice attempts at fitting the ion fractions on the basis of a simple formula based only on the dependence on the perpendicular velocity were not successful (Maazouz *et al* 1998). Furthermore the aforementioned 'parallel velocity' effect required an explanation.

Since the Si target can hardly be described within the free-electron model, the 'shifted Fermi sphere' based discussion of electron capture and 'parallel velocity' effect is not appropriate here. In order to explain the parallel velocity dependence of the ion fractions at grazing scattering angles, Maazouz *et al* (1997, 1998) proposed an alternative description

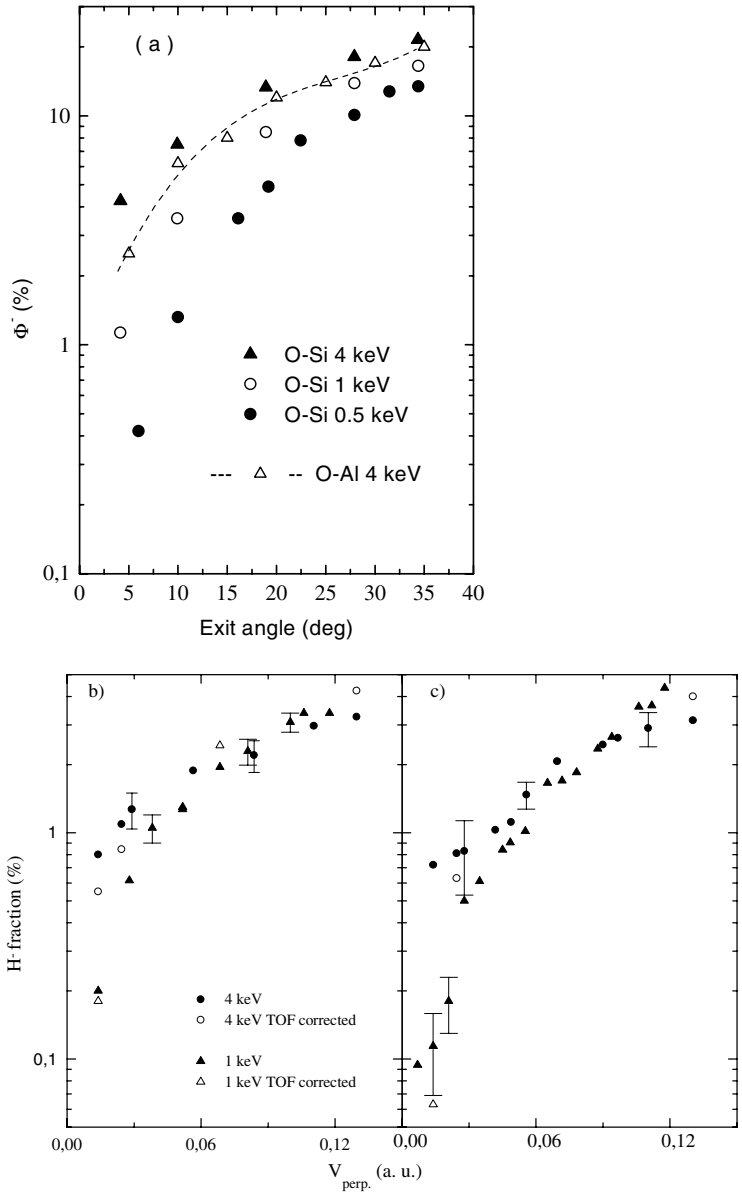

Figure 2. (a) O^- ion fractions for oxygen anion scattering on Si (Maazouz *et al* 1987) and Al (Maazouz *et al* 1987). (b), (c) H^- ion fractions as a function of perpendicular velocity for (b) Si (Maazouz *et al* 1987, 1988) and (c) Al (Maazouz *et al* 1986) for 1 and 4 keV incident ion energies.

related to the specific features of the electronic structure of the Si surface. The surface LDOS is characterized by the appearance of the rather well localized dangling bond states at the top of the valence band and in the gap region. Calculations for the Si(100) (Ciraci *et al* 1984), Si(111) (Qian and Chadi 1987) and amorphous Si (Biswas *et al* 1989) surfaces all indicate the presence of narrow bands of surface states at an energy position close to the top of the bulk valence band region. The DOS of the outermost Si layers is schematized in figure 1(b) for

the Si(100) surface on the basis of some existing model calculations (Ciraci *et al* 1984). The existence of this band, due to the Si surface atoms suggested a model of *non-resonant electron capture* on the same lines as the non-resonant charge transfer processes in gas-phase collisions by Demkov (1964) (see also Olson 1972, Nikitin 1962, Nikitin and Umanskii 1984). For the Si case, this corresponds to non-resonant charge exchange involving the affinity level of the projectile and the narrow band of surface states. The idea of the model is somewhat similar to the case of the ionic solids described below (e.g. equation (11)). Note that in the case of Si a resonant charge transfer process involving these surface states has been invoked to explain oscillations in the energy dependence of excited state population in Si^{+*} sputtering (Ledyankin *et al* 1988, 1990) as well as O^{2-} formation in scattering from the Si surface (Rechtein *et al* 1990). For a given energy defect (ΔE), the probability of non-resonant electron transfer increases strongly with velocity (v) in the low (threshold) velocity region (see equation (11) below). This could qualitatively explain the observed velocity dependence in grazing, distant atom–surface, conditions. The existence of resonant capture and loss processes involving bulk valence band and conduction band states should of course also be taken into account in order to perform quantitative analysis of experimental data. It has been suggested (Maazouz *et al* 1998) that also in the case of diamond, such surface states (Scholze *et al* 1996a, b) could also play a role in negative ion formation leading to large ion fractions.

Importance of dangling bonds on the negative ion formation has also been pointed out by Morris *et al* (1995). They studied the O^- ion yield in dissociating collision of hyperthermal NO^+ with the GaAs(110) surface. A marked angular dependence of the O^- emergence was found and explained by a localized nature of the charge transfer process. Basically, it was argued that O^- formation occurs predominantly for oxygen atoms which come in close contact with the localized dangling bond states of GaAs(110).

4. Experimental studies of negative ion formation on ionic solids

An elegant series of experiments dealing with measurements of energy spectra of backscattered ions in H^+ and He^+ scattering have been reported by Souda *et al* (1992, 1993a, b, 1995, 1999a, b) for various insulating surfaces (oxides, alkali halides etc). It was shown that resonant neutralization of H^+ occurs quite efficiently. The H^+ level is resonant with the O(2p) level in e.g. MgO and with halide anion levels in a number of alkali halides. This result may therefore not appear to be very surprising. However a very interesting finding, was that of *backscattered* H^- for low collision energies (around 50 to 100 eV). Examples of backscattered positive and negative ion spectra are shown in figure 3 for 100 eV H^+ incident ions for the case of a LiCl surface (Souda *et al* 1995). Similar results are obtained for oxidized Mg and bulk MgO (Souda and Yamamoto 1997, Souda 1997). The spectra clearly display single scattering peaks of H^+ and also H^-. This shows that even though on the energy level diagram (figure 1(b)) the situation looks very unfavourable, electron capture does occur.

Another important feature, which distinguishes these results clearly from those for clean metal surfaces, was the observation of a *site-specific character* of neutralization. Thus in figure 3 the backscattered H^+ intensity was higher for backscattering off chlorine than off lithium. Similar results were reported for MgO. Souda *et al* (1995) concluded that H^- was formed predominantly on the cation site in H^+ scattering. These experiments thus clearly delineate the localized, site-specific, nature of the electron capture process, consistent with the localized nature of charges in these ionic solids. Capture probabilities could not be determined by Souda *et al*, since the neutral particle flux was not monitored.

Stracke *et al* (1997) studied emission of electrons in slow collisions (50 to 500 eV) of N^+ ions with LiF and CsI films deposited on a tungsten support (see also the review paper

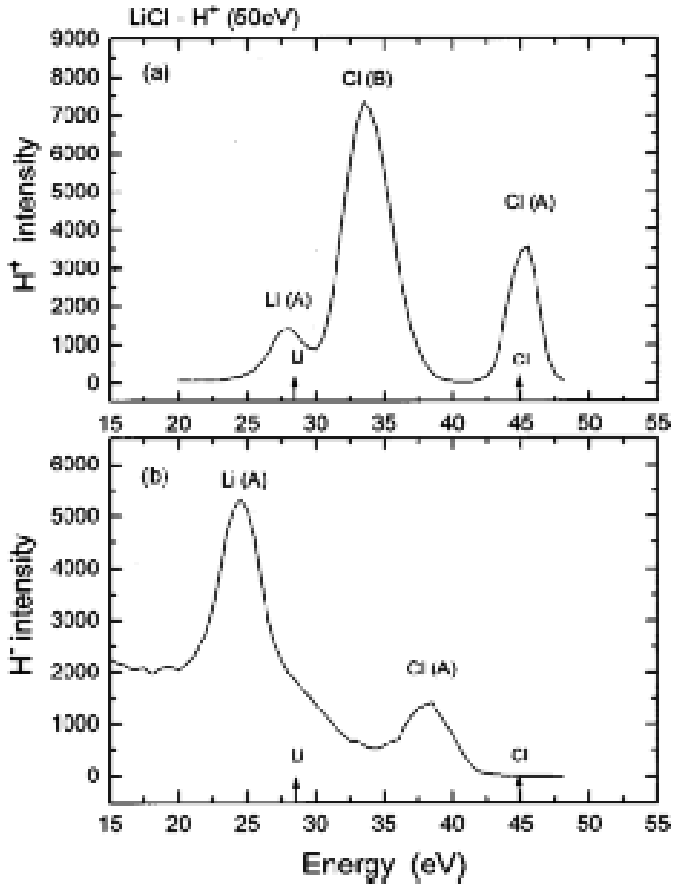

Figure 3. Data of Souda *et al* for H^+ scattering on LiCl (after Souda *et al* 1995, with permission). (a) H^+ energy loss spectra and (b) H^- energy loss spectra.

by Kempter (1998)). They found that the electron spectra display a sharp feature on top of a smooth continuous background. This feature was attributed to autodetachment of $N^{-*}(2p^4; {}^1D)$ temporary ions to the $N^0(2p^3; {}^4S)$ ground state atoms. It was argued that the formation of metastable negative ions proceeds in two steps. First, the N^+ projectiles are neutralized possibly in all three multiplet states ^4S, ^2D, and ^2P of the $N^0(2s^22p^3)$ configuration. As a second step, the $N^{-*}(^1D)$ metastable ion is formed by electron attachment to $N^*(^2D)$. In fact, formation of metastable $N^{-*}(^1D)$ ions was also observed in N^+ interactions with metal surfaces (tungsten) covered with alkali adsorbates (Müller *et al* 1994, 1996, Bahrim *et al* 1997). The efficiency of the negative ion formation was estimated to be comparable on alkali halide and metal surfaces. This is a very spectacular result keeping in mind that alkali adsorbates were used to reduce the work function and facilitate the negative ion formation in the metal case while the binding energies of the valence band electrons of the ionic materials are in the 10 eV domain (figure 1(b)).

More quantitative information, showing that electron capture occurs efficiently on ionic crystals, has come from studies of negative ion formation on alkali halides (e.g. Auth *et al* 1995a, 1998b, Auth 1996, Winter *et al* 1996a, b, 1999, Meyer *et al* 1997), oxidized Mg and Al surfaces (Shi *et al* 1989, Maazouz *et al* 1996, Esaulov *et al* 1997, Ustaze *et al* 1997b, c,

1998) and MgO (Ustaze *et al* 1997b), and the Ag(111) surface exposed to Cl_2 (Casagrande *et al* 2000).

Maazouz *et al* (1996), Esaulov *et al* (1997) and Ustaze *et al* (1997b, c, 1998) investigated formation of negative ions in scattering from Mg and Al surfaces exposed to oxygen. Note that at high exposures (for Mg this corresponds to doses above about 5 Langmuir (L) units, $1\ \mathrm{L} = 10^{-6}$ Torr s), the surface electronic structure resembles that of an oxide (figure 1(b)) and displays a well developed bandgap (see e.g. Ustaze *et al* 1997c). High exposures result in the formation of an oxide film of a few Ångströms thickness (Fuggle 1977). The experiments consisted in the measurement of the negative (Φ^-) ion fractions. A typical result for H^- and O^- formation on an Mg surface exposed to increasing doses of oxygen is shown in figure 4(a). For grazing exit angles (3.5°) the negative ion yield is quite small for a clean Mg surface, but as the surface is exposed to oxygen the yield increases substantially and reaches a broad plateau at high exposures. Similar results were obtained on oxidized Al. A large ion fraction for F^- formation has been observed on oxidized Mg (Ustaze *et al* 1997c, 1998). These measurements thus clearly indicated that on a surface covered with a thin oxide film, negative ion formation occurs with a high probability.

Recently Casagrande *et al* (2000) investigated F^- backscattering on Ag(111) exposed to increasing doses of Cl_2, from the sumonolayer chemisorption to AgCl formation stages. An interesting feature of these experiments was that their ISS spectra show F^- scattered off Cl on the surface only for *high* coverages (figure 4(b)), in this case above 1.5 L) corresponding to AgCl formation (see e.g. Andryushechkin *et al* 1998 and references therein). In the same exposure range, ion fraction measurements for grazing scattering showed initially a decrease in the F^- ion fraction in submonolayer *chemisorption* stages and then a sudden increase when AgCl islands start to form (above 1.5 L, figure 4(c)). These experiments demonstrate a specific local character of the electron transfer process on the dielectric layer, which is of a different nature from the case of chemisorbed atoms.

In order to confirm the results of experiments on oxidized surfaces, a series of experiments using both neutral and negative ion incident beams were performed on a bulk oxide MgO(001) surface in order to study both electron capture and electron loss processes (Ustaze *et al* 1997b). Results of Ustaze *et al* (1997b) are shown in figure 4(d). For incident *neutral* particles the ion fractions increase rapidly from a threshold in the energy range of a few hundred eV to a rather large value for energies of a few keV. A very large ion fraction is obtained on the oxide surface using incident atoms (7%, 35% and 75% for H^-, O^-, F^-), indicating that electron capture can occur most efficiently. As a comparison, in a similar scattering geometry for H^- and O^- scattering on a clean Mg surface, an ion fraction of only 1% (Maazouz *et al* 1996; see also figure 2) and 10% (Maazouz *et al* 1997) respectively was found for 4 keV, while for MgO the corresponding fractions are much larger. Some preliminary measurements (Ustaze *et al* 1997a) conducted on a bulk Al_2O_3 sample also indicated that significant capture occurs.

An equally important observation of these experiments, using an incident negative ion beam, was that of the existence of an electron loss process. Rather different behaviours are observed for the studied systems. For H^- the negative ion yield is similar for incident H and H^-. For F^- reflection of the negative ions is complete for low energies. As the energy increases, the F^- ion fraction decreases and for energies of the order of 1.5 keV, results for incident ions and neutrals become identical within the limits of statistical error. For O^- an intermediate situation is encountered. At low energies the ion fraction for incident O^- is somewhat larger than for incident O atoms.

Extremely efficient negative ion formation was observed for the alkali halide targets (Auth *et al* 1995a, 1998b, Winter *et al* 1996a, b, 1999, Meyer *et al* 1997). Figure 5(a) displays the

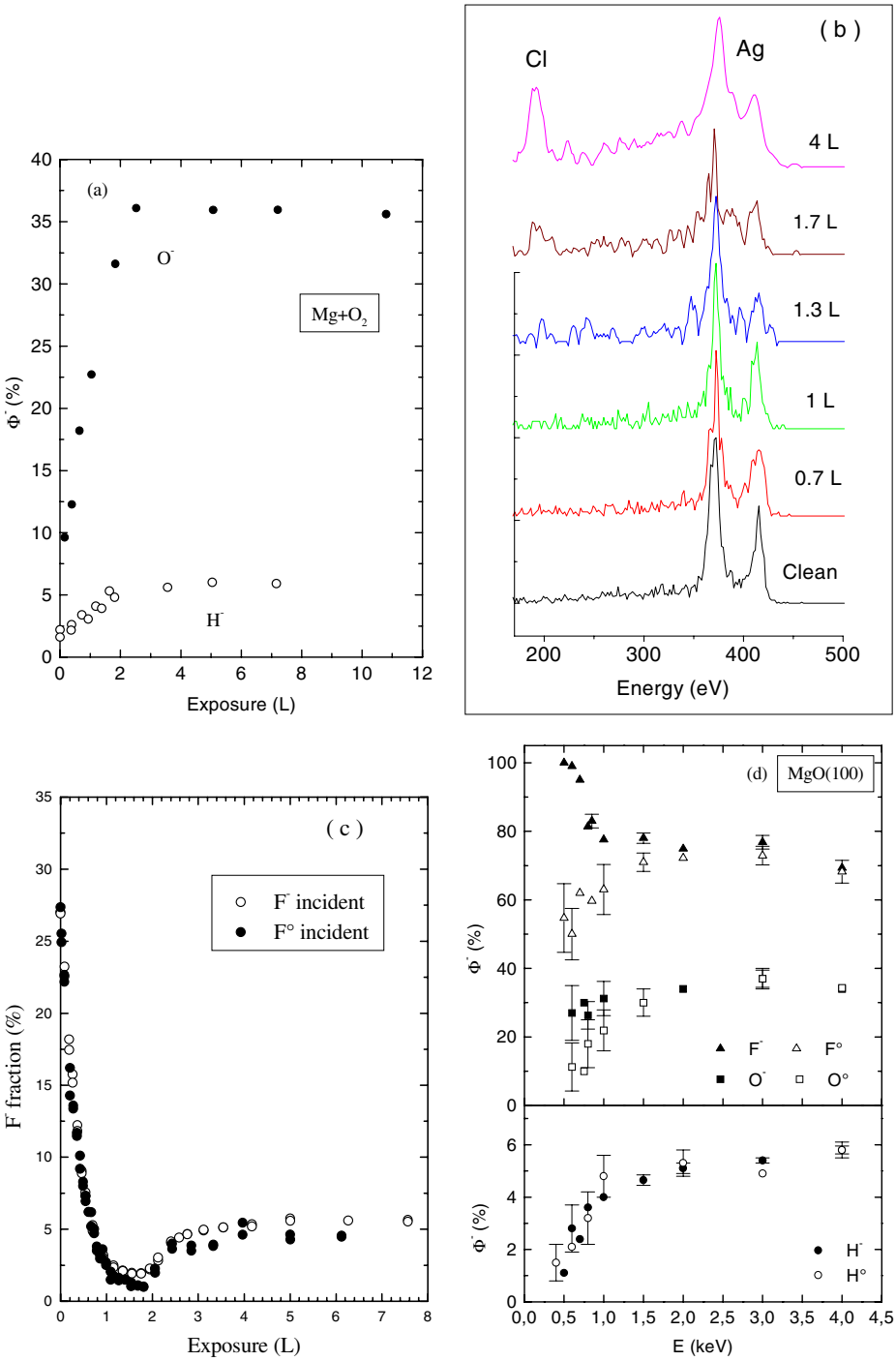

Figure 4. (a) Variation of the H^- and O^- fraction as a function of oxygen exposure on Mg for a 4 keV incident ion energy. (b) Energy spectra of F^- backscattered on an Ag(111) surface as a function of Cl_2 exposure (from Casagrande *et al* 2000). (c) Ion fractions for F^- formation in grazing scattering on an Ag(111) surface as a function of Cl_2 exposure (from Casagrande *et al* 2000). (d) Negative ion fractions obtained in the scattering of H, O and F atoms on MgO(100). In both cases the data correspond to grazing specular scattering (3.5°) conditions (adapted from Maazouz *et al* 1996 and Ustaze *et al* 1997b).

results of Auth *et al* (1998b) for F^-, O^- and H^- formation on an LiF(001) surface as a function of ion velocity for grazing scattering conditions (incidence angles less than 1°). A spectacular feature of these results is the almost 90% F^- and 60% O^- ion fractions in the scattered beam. Note, that only 6% O^- ions are found for grazing scattering from Al(111) (Auth *et al* 1998c) and Au(110) (Folkerts *et al* 1995) surfaces in similar scattering conditions. In general bell shaped curves are obtained with a low energy threshold for the negative ion formation and a decrease in the ion fraction at high energy. The negative ion fractions decrease with decreasing electron affinity. The threshold for capture is lower for the more strongly bound F^-.

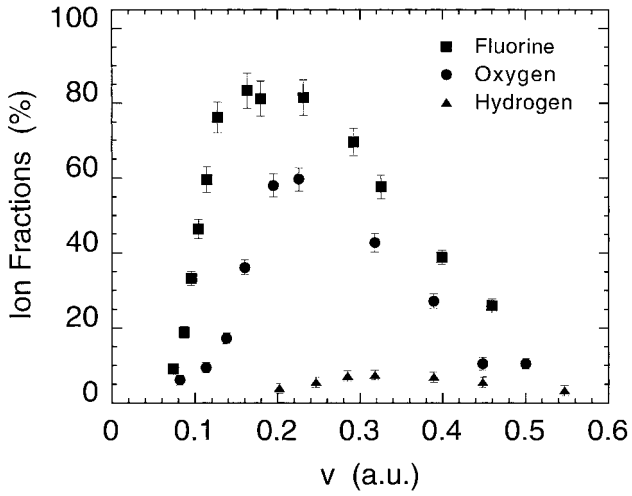

(a)

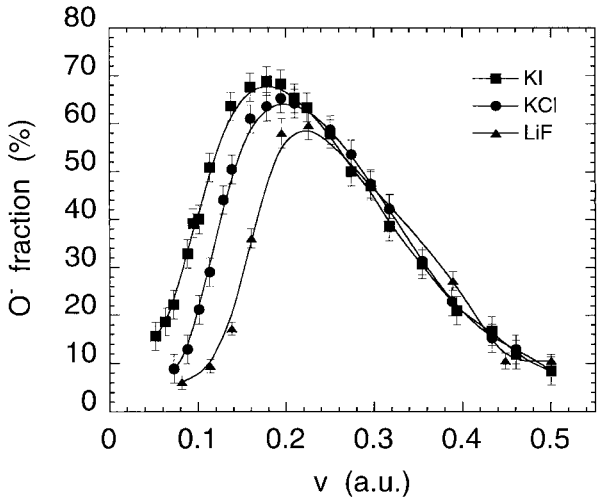

(b)

Figure 5. (a) Negative ion fractions as functions of projectile velocity for hydrogen, oxygen and fluorine atoms scattered from LiF(001). The incidence angle of the scattered beam is 1° as measured from the surface plane. (from Auth *et al* 1998b). (b) Negative ion fractions as functions of projectile velocity for oxygen atoms scattered from KI, KCl, and LiF(001) surfaces. The incidence angle of the scattered beam is 1° as measured from the surface plane. Solid lines are drawn to guide the eye (from Auth *et al* 1998b).

Figure 5(b) shows experimental data for O^- formation on different alkali halide surfaces (LiF(001), KCl(001), KI(001)) as a function of ion velocity for the same scattering conditions as in figure 5(a). As may be seen, the magnitude of the negative ion fraction is the largest for the KI(001) surface, while it is the smallest for the LiF(001) surface. The negative ion formation threshold shifts towards smaller velocities for the LiF–KCl–KI sequence. The bell shape of the curves is observed for all three surfaces with lowering of the O^- fraction towards high velocities. It is worth mentioning that for the KI(001) target saturation of the F^- fraction at almost a 100% level was obtained (Winter *et al* 1996b).

Measurements of energy losses in large angle scattering of H^+ on LiCl and some other compounds (Souda *et al* 1995, 1998, 1999a, b) and recent studies of the energy losses experienced by the 0.5–4 keV hydrogen projectiles grazingly scattered from the LiF(001) surface (Auth *et al* 1998a, Roncin *et al* 1999), show the existence of discrete structures in the energy loss spectra. Thus for LiCl, Souda *et al* (1995, 1998) observed that H^- formation is accompanied by an energy loss of about 7 eV (see figure 3(b)) consistent with LiCl valence band excitation. Similar results were found for other compounds (Souda *et al* 1998, 1999b). For LiF energy loss structures separated by approximately 12 eV were found (Roncin *et al* 1999, see figure 6). This indicates that the projectile–surface interaction is accompanied by a series of excitations of LiF valence electrons, where approximately 12 eV is needed to bring the valence band electron into the H^- affinity level, into the vacuum or into the surface exciton states.

Analysis of the energy loss spectra of the H and H^- scattered species taken in coincidence with emitted electrons allowed a number of important findings (Roncin *et al* 1999, Villette *et al* 1999). It was demonstrated that the hydrogen projectile experiences a number of electron capture–loss cycles along its trajectory near the surface. The H^- ion formed in the course of the capture event is an extremely efficient intermediate in bringing LiF valence band electrons into the vacuum states (electron emission), and in populating the surface exciton states. The probability of electron capture (loss) per visited unit cell at the surface on the 15% (40%) level was evaluated from the fit to the experimental data.

All these experiments clearly show that charge transfer at the insulating surfaces of ionic crystals (oxides, alkali halides) is characterized by very efficient electron capture leading to the large negative ion yields in the scattered beam, even though the disposition of the energy levels looks *a priori* very unfavourable. The existence of an electron loss process was demonstrated. As a result of the electron capture-then-loss cycles negative ions play an important role in bridging the energy gap between the valence band states and excited states, and, in particular, in electron emission.

5. Descriptions of negative ion formation on ionic solids

We shall now briefly summarize the different models used to explain experimental observations.

5.1. Low energy scattering

The ionic solids (alkali halides, MgO) are characterized by the localization of the charges at the crystal sites. Consider, for example, the case of the alkali halide crystals. They consist of positively charged alkali-metal ions (Alk^+) and negatively charged halogen ions (Hal^-) at lattice sites. The valence band originates from the $Hal^-(np_{x,y,z})$ orbitals and the valence band electrons are localized at the Hal^- sites (Kunz 1975, Zunger and Freeman 1977, Tatewaki and Miyoshi 1995, Wertheim *et al* 1995). A detailed discussion of oxides may be found in the book by Noguera (1996). The binding energies of the valence-band electrons can be well

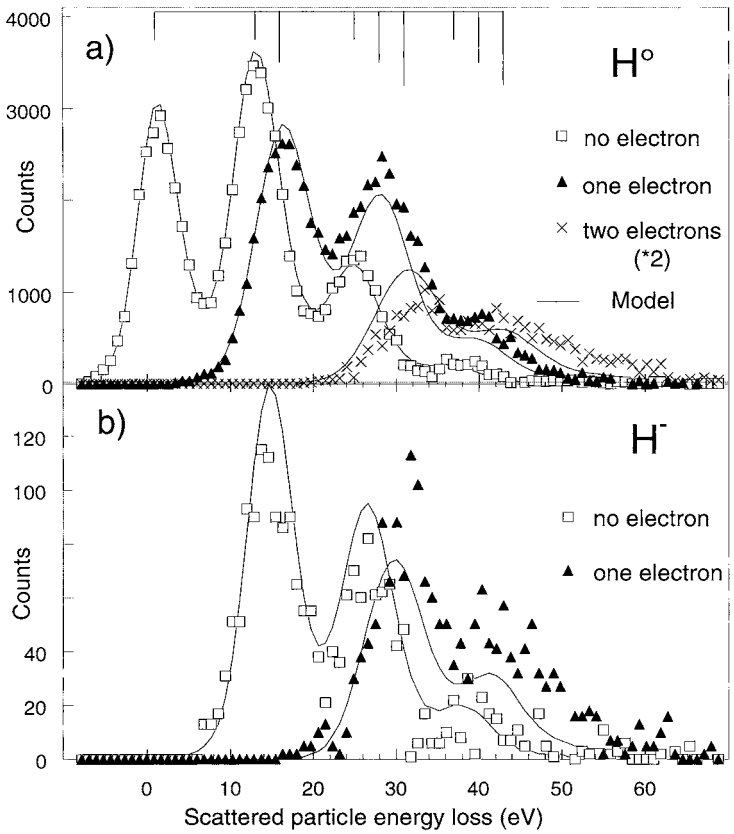

Figure 6. Energy loss spectra of scattered H° and H^{-} grazing scattering on LiF, associated with the emission of no electrons and one or two electrons. The full curve is a fit from a model of electron-loss cycles undergone by the H projectile. The vertical lines indicate the peak positions (after Roncin *et al* 1999).

approximated by the affinity of the free Hal^{-} ion increased by the Madelung potential: the potential created by the rest of the ions in the crystal, treated as point charges, on a halogen site. Other contributions come from the finite valence band width and from the polarization (Mott and Littleton 1938, Mahan 1980) effects.

In an attempt to explain their observations of H^{+} neutralization and H^{-} formation in low energy backscattering on alkali halides and oxides, Souda *et al* (1998, 1999b and references therin) used these properties of ionic crystals and performed molecular orbital (MO) calculations for small clusters (e.g. $(LiCl_5)^{4-}$ or $(ClLi_5)^{4+}$) with H^{+} located top of either the alkali cation or the Cl anion. The electron capture was discussed in terms of the adiabatic behaviour of the MO correlated with the H(1s) atomic orbital at large separations from the cluster. It was found that at small distances from anions the H(1s) orbital had an antibonding character and was promoted or shifted upwards to higher energies, while for the cations it remained close or resonant with the highest occupied molecular orbital corresponding to the anion levels. In the anion site case a loss of H(1s) character was observed, while it was partly retained in the cation-site case. Thus it was concluded that e.g. H^{+} neutralization by resonant capture would occur predominantly on the cation site, in agreement with experiment. Negative ion formation was also discussed in this framework and the authors reported an

occupancy of the H(1s) level greater than unity for the $(LiCl_5)^{4-}$ cluster case. Souda *et al* (1998, 1999b) point out that amphoteric hydrogen is coordinated negatively (positively) on cation (anion) sites, and in low energy collisions hydrogen retains the memory of its 'transient chemisorption' state. It is however important to realize that even though electron capture might proceed at the positively charged lattice site, the captured electron is a valence band electron, i.e. it comes from the anion (Hal^-, O^{2-}) site at the surface. It seems reasonable to suppose that in these experiments two electron capture ($H^+ \rightarrow H^-$) would occur more easily on a cation site surrounded by several anions which can contribute electrons, rather than on an anion site.

Souda *et al* (1995, 1998, 1999a, b, Souda and Yamamoto 1997, Souda 1997) proposed this MO picture as a tentative explanation of the observed charge fractions in the backscattered beams. At the same time it should be noted that the projectile–surface charge-transfer process is essentially a nonadiabatic dynamic phenomenon. Therefore a dynamical approach is needed to understand the basic physics underlying charge transfer processes on the ionic crystal surfaces.

Such a dynamical treatment of the H^+ neutralization and H^- formation in backscattering from the LiF(001) surface was performed recently by García *et al* (1999) within the time-dependent Hartree–Fock method and with use of the Green function technique. The LiF(001) surface was represented by a cluster $(F_5Li)^{4-}$ or $(Li_5F)^{4+}$, depending on the collision geometry (backscattering from the Li^+ or F^- site, respectively). The cluster was imbedded in the ionic cage to account for the Madelung potential of the crystal. Enhanced H^- formation was observed in backscattering from the cation (Li^+) sites of the surface compared to backscattering from the anion (F^-) sites. This is in agreement with experimental observations of Souda *et al* (1995, 1998, 1999a, b, Souda and Yamamoto 1997, Souda 1997). It was found that the short range interactions with the nuclei and electrons of the target determine mainly the mechanism of the charge exchange in this case.

5.2. Capture and loss in fast grazing scattering

5.2.1. General outline. As opposed to backscattering experiments a grazing scattering geometry is characterized by small angles between the incident beam and the surface. The projectiles are then 'softly' scattered, without violent collisions with target atoms. The trajectory path close to the surface is very long so that the projectile interacts with a large number of surface sites compared to preferentially one surface site in the backscattering experiments. The negative ion fraction in the scattered beam results from the interplay between electron capture and electron loss processes. Ionic crystals are characterized by the large bandgap that *a priori* reduces the electron losses by removing the electronic states of the target in resonance with the affinity level of the projectile. Indeed, as one can see in figure 1(b), the F^- and O^- affinity levels are situated within the bandgap so that there are no electronic states of the surface available for the electron transfer from the negative ion. In case of H^- only the states close to the bottom of the conduction band can participate in the negative ion destruction via the resonant electron transfer process. This explains why, once formed, negative ions have a large probability to survive during the collision with an ionic crystal surface. At the same time one has to answer the question: how can negative ions be formed with high efficiencies despite the large energy difference between the affinity levels and occupied valence band states of the target surface? In what follows below we will address this point.

It is tempting to explain the large negative ion fractions in the outgoing beam by the presence of occupied states with low binding energies at the surface of the ionic crystal (Meyer *et al* 1997). In this case negative ion formation would proceed via resonant electron capture from these states. However this model contradicts other experimental data available on charge

transfer at the surfaces of ionic crystals. Indeed, the experiments on alkali-metal ion scattering from the surfaces of alkali halide crystals demonstrate that there are no surface states with binding energies comparable to the ionization potentials of alkali-metal atoms (Winter *et al* 1997, Mertens *et al* 1997). Note that binding energies of negative ions (electron affinities) are in the same range as ionization potentials of alkali-metal atoms. Furthermore, a suppression of Auger electron capture was observed for He^+ and Ne^+ projectiles in the scattering from a LiF(001) surface (Hecht *et al* 1996). This can only be explained by the large binding energies of the valence band electrons and would not be possible if occupied states with low binding energies were present with sufficient density at the surface. In fact, such surface states are found neither in metastable helium deexcitation spectroscopy (Wiegershaus *et al* 1996) nor in *ab initio* band-structure calculations (Wu *et al* 1995).

A binary-type charge transfer model, based on the localized character of the charges in an ionic solid has been proposed to describe the negative ion formation in grazing scattering of F, O and H projectiles from alkali halide surfaces (Auth *et al* 1995a, 1998b, Borisov *et al* 1996, Borisov and Sidis 1997). In fact, this model can be easily applied for the MgO target with minor modifications resulting from the Mg^{2+} and O^{2-} charges of the ions at the lattice sites (Deutscher *et al* 1999a, b). (For the charges in the MgO ionic lattice see e.g. Sousa *et al* 1993, Illas *et al* 1993, Brudevoll *et al* 1996, Zuo *et al* 1997.) It is worth mentioning that recent developments of the theoretical descriptions of the neutralization of multicharged ions interacting with ionic crystal surfaces (Hägg *et al* 1997, Ducrée *et al* 1998) emerge from the same physical principles though description of the dynamics of electron transfer is different.

Consider electron capture by a projectile A^q, of charge q, from the surface of an ionic crystal. It involves valence-band electrons localized at the Hal^- crystal sites. Therefore one deals with *localized electron capture* that can be viewed as a series of binary interactions between the projectile and Hal^- ions at the crystal sites as sketched in figure 7 (Borisov *et al* 1996, Borisov and Sidis 1997)

$$Hal^- + A^q \rightarrow Hal^0 + A^{q-1}. \tag{1}$$

In each of these binary interactions we have an *active site*: the site actually participating in the charge transfer process. Other ions of the crystal are spectators and are considered as point charges. Note that owing to the flat and narrow valence band of ionic crystals, the hole mobility is low: i.e., the removal of an electron from a Hal^- site leaves the corresponding hole localized at that site on the time scale of the collision (Mahan 1980, Ducrée *et al* 1998).

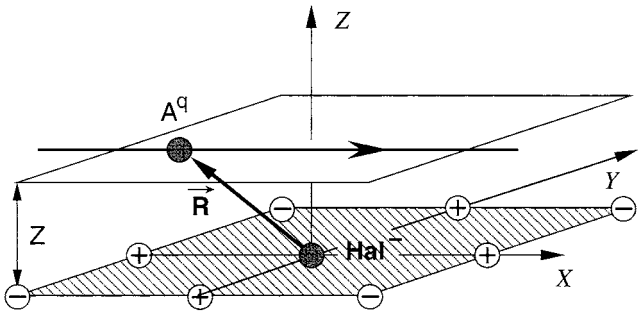

Figure 7. Sketch of the considered binary interaction model. The shaded plane represents the portion of the last layer of the ionic surface surrounding a Hal^- active site (dark central circle). Circled $\pm$ symbols represent mere point charges. The straight line at distance Z from the surface shows the trajectory of the impinging A^q projectile (dark upper circle) as it passes by. (Adapted from Borisov and Sidis 1997).

5.2.2. Energy level confluence. The efficiency of the electron-transfer mechanism is determined by the energy difference between initial ($Hal^- + A^q$) and final ($Hal^0 + A^{q-1}$) diabatic states during the collision:

$$\Delta E(\vec{R}) = E(\mathrm{Hal}^0 + \mathrm{A}^{q-1}) - E(\mathrm{Hal}^- + \mathrm{A}^q). \tag{2}$$

$\Delta E(\vec{R})$ is the energy that is needed to move an electron from the Hal^- ion at the surface to the projectile located at $\vec{R}$ (figure 7).

For simplicity we will neglect polarization effects including image potentials. In addition we will consider a range of distances $R \equiv |\vec{R}|$ between the projectile and the active site large enough so that the electronic clouds of the Hal^- at the active site and the projectile do not overlap significantly. With these approximations we have:

$$E(\mathrm{Hal}^- + \mathrm{A}^q) = E_{Hal^-} + E_{A^q} + \frac{1}{2}\sum_{i\neq j}\frac{q_i q_j}{|\vec{r}_i - \vec{r}_j|} - \sum_i \frac{q_i}{|\vec{r}_i|} + \sum_i \frac{q q_i}{|\vec{R} - \vec{r}_i|} - \frac{q}{R}. \tag{3}$$

In equation (3) the summations run over point charges, i.e., *excluding the active site.* E_{Hal^-} and E_{A^q} are the total energies of the free Hal^- ion and projectile A^q, respectively. The $q_i = \pm 1$ are the point charges at the crystal sites located at $\vec{r}_i$ with respect to the active site. The third term gives the interaction energy between the point charges. The fourth term is the interaction energy between the active site (having a charge -1) and all other sites of the crystal. The fifth term is the interaction energy between the projectile and the point charges. Finally, the last term is the interaction energy between the charge of the projectile and that of the active site. Similarly,

$$E(\mathrm{Hal}^0 + \mathrm{A}^{q-1}) = E_{Hal^0} + E_{A^{q-1}} + \frac{1}{2}\sum_{i\neq j}\frac{q_i q_j}{|\vec{r}_i - \vec{r}_j|} + \sum_i \frac{(q-1)q_i}{|\vec{R} - \vec{r}_i|}. \tag{4}$$

Equation (4) takes into account the fact that the removal of the electron from the active site leaves a null charge at this site. Note that in case of the charge transfer on the MgO surface removal of the electron from the active site leaves a -1 charge at this site (initial charge state O^{2-}). From equations (3) and (4) we obtain the energy difference:

$$\Delta E(\vec{R}) = \varepsilon_{Hal^-} - \varepsilon_{A^{q-1}} + \sum_i \frac{q_i}{|\vec{r}_i|} - \sum_i \frac{q_i}{|\vec{R} - \vec{r}_i|} + \frac{q}{R} \tag{5}$$

where $\varepsilon_{Hal^-} = E^0_{Hal} - E_{Hal^-}$ and $\varepsilon_{A^{q-1}} = E_{A^q} - E_{A^{q-1}}$ are the binding energies of the electron in the free Hal^- ion and free A^{q-1} projectile, respectively. The last two terms give the difference between the Madelung potentials created by the point charges at the Hal^- site ($E_{Mad}(0) \equiv E_{Mad}$) and the point $\vec{R}(E_{Mad}(\vec{R}))$. So, finally equation (5) can be rewritten as:

$$\Delta E(\vec{R}) = \varepsilon_{Hal^-} - \varepsilon_{A^{q-1}} + E_{Mad} - E_{Mad}(\vec{R}) + \frac{q}{R}. \tag{6}$$

As already stated, in derivation of equations (3)–(6) point charges of the crystal lattice were assumed to be unpolarizable in order to keep the discussion simple. In fact, effects due to the polarization of the point charges (Mott and Littleton 1938) can be easily incorporated into the treatment by including terms corresponding to the interaction energy between the induced dipole and the field (Mahan 1980, Borisov and Sidis 1997, Hägg *et al* 1997, Ducrée *et al* 1998).

Let us consider the case $R \gg a$ where a is the lattice constant. For a distant charge, a hole created on the neutral crystal by removal of the electron from the active site is seen as $a + 1$ charge. So, $E_{Mad}(\vec{R}) \approx 1/R$ and equation (6) transforms to:

$$\Delta E(\vec{R}) = \varepsilon_{Hal^-} - \varepsilon_{A^{q-1}} + E_{Mad} + \frac{q-1}{R}. \tag{7}$$

Intuitively, the meaning of equation (7) is quite clear. Initially we had an electron at the Hal^- crystal site and the A^q projectile in front of the *neutral* crystal. So, except for polarization effects, the relevant energy is given by the energy of the electron attached to the Hal^- ion: $E_{Initial} = -E_{Mad} - \varepsilon_{Hal^-}$ ($E_{Initial}$ can also be estimated from the energy of the centre of the valence band with respect to the vacuum level). The final state corresponds to the electron located at the A^{q-1} projectile in the presence of the hole (at the origin of coordinates) on the crystal. This hole is equivalent to a positive charge at $R = 0$. The corresponding energy is $E_{Final} = (q-1)/R - \varepsilon_{A^{q-1}}$. The first term gives the interaction of the A^{q-1} projectile with the hole at the surface. The second term corresponds to the energy of the electron level of the A^{q-1} projectile. Equation (7) is just the $E_{Final} - E_{Initial}$ difference.

Let us consider the case of the negative ion formation from the neutral projectile ($q = 0$). Equations (6) and (7) become respectively:

$$\Delta E(\vec{R}) = \varepsilon_{Hal^-} - \varepsilon_{A^-} + E_{Mad} - E_{Mad}(\vec{R}) \tag{8}$$

and

$$\Delta E(\vec{R}) = \varepsilon_{Hal^-} - \varepsilon_{A^-} + E_{Mad} - \frac{1}{R}. \tag{9}$$

Equation (9) pinpoints the basic phenomenon that initiates a confluence of the relevant energy levels and therefore enables the electron capture from the halogen sites. It is essentially due to Coulomb interaction in the final state between the negative projectile and the hole created in the neutral crystal by the removal of an electron. Note that in case of the neutralization of the positively charged ion ($q = +1$) the confluence mechanism is not active (see equation (7)). This qualitatively explains the results of Winter *et al* (1997) and Mertens *et al* (1997). Namely, despite similar binding energies of the electron in the F^- ion and Na atom, in the range of the projectile velocities where F atoms grazingly scattered from a LiF(001) surface are efficiently transformed into F^- ions, Na^+ projectiles remain un-neutralized.

In figure 8 we show $\Delta E(\vec{R})$ calculated from equation (8) for F^- formation at LiF(001) and KI(001) surfaces ($\varepsilon_{F^-} = 3.4$ eV, and $\varepsilon_{I^-} = 3.37$ eV where the spin–orbit interaction in the neutral I atom is removed). We consider a part of the trajectory of the projectile close to

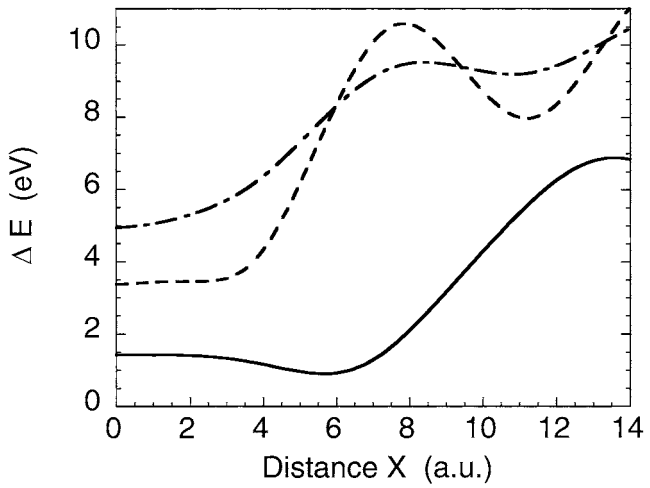

Figure 8. Behaviour of the energy difference ΔE between final and initial states for F^- formation at KI(001) (solid line) and LiF(001) (dashed and dashed–dotted lines) surfaces. The projectile–surface distance Z is 2.5 au (dashed line) and 3.5 au (solid and dashed–dotted lines).

the turning point and therefore parallel to the surface: $\vec{R}(t) = (X = vt, 0, Z)$, where v is the projectile velocity. The scattered beam is assumed to be parallel to the $\langle 100 \rangle$ direction. Only positive values of the X coordinate are shown. The case $Y = 0$ corresponds to the passage 'on top' of the active site at the surface. The calculations show that ΔE decreases essentially as soon as the active site is approached. This facilitates electron transfer from the active site to the projectile.

An important feature seen in figure 8 consists in a remarkable difference between F^- formation at LiF(001) and KI(001) surfaces. Indeed, for the same ion–surface distance Z the energy defect for the charge transfer ΔE is much smaller in the case of the KI(001) surface. This can be explained by the larger lattice constant of the KI crystal ($a = 13.34\, a_0$) compared to LiF ($a = 7.59\, a_0$). As it follows from equation (8), the energy difference ΔE is governed by the difference of the Madelung potentials at the active site and the position $\vec{R}$ of the projectile. Since the characteristic size of the variation of the Madelung field is given by the lattice constant a, the smaller the ratio R/a, the smaller the difference $E_{Mad} - E_{Mad}(\vec{R})$. For the same reasons a reduction of the projectile–surface distance Z leads to the reduction of ΔE.

5.2.3. Population build-up. Consider a projectile grazingly scattered along the $\langle 100 \rangle$ direction of the LiF(001) surface. Owing to the small angle of the scattered beam with respect to the surface plane one can consider that during its binary encounter with an active site the projectile moves along the trajectory parallel to the surface (figure 7). To obtain the probability of the electron transfer process (equation (1)) during the binary collision with an active site the following procedure can be applied (Borisov and Sidis 1997). First, one calculates electron transfer probabilities $P(Y, Z)$ along a set of straight line trajectories $\vec{R}(t) = (X = vt, Y, Z)$. Then, the final transition probability $P^{site}(Z)$ in a binary collision with an active site can be obtained by averaging $P(Y, Z)$ over trajectories in the Y range $[-a/2, a/2]$ spanning a region of impact parameters per active site in the $\langle 010 \rangle$ direction. $P^{site}(Z)$ gives the probability of the conversion to negative ions of a beam of neutral projectiles lying in an XY plane, at distance Z from the surface, and travelling along the $\langle 100 \rangle$ (X) direction, when crossing a row of surface atoms oriented along the $\langle 010 \rangle$ (Y) direction perpendicular to the beam.

Projectiles scattered in the $\langle 100 \rangle$ direction cross successive rows of surface atoms oriented in the $\langle 010 \rangle$ direction at X_i points separated by $a/2$. If one completely neglects the electron loss process, the final negative ion yield can be evaluated as

$$P^{total} = 1 - \prod_{i=1}^{N} \{1 - P^{site}(Z_i)\} \tag{10}$$

where $Z_i = Z(X_i)$ when $Z(X)$ is the trajectory of the scattered projectile lying in the plane normal to the surface.

Equation (10) provides a *quantitative* description of the charge transfer process. At the same time it requires a knowledge of the charge transfer probabilities $P(Y, Z)$ which can be obtained only on the basis of parameter free calculation of the binary charge transfer process. A much simpler scheme can be applied for the *qualitative* analysis of the experimental results. As we have seen in figure 8, the energy difference ΔE is almost constant over the charge transfer region (close to the active site). Therefore one can apply the Demkov–Nikitin near-resonant electron-transfer model (Nikitin 1962, Demkov 1964, Nikitin and Umanskii 1984) to describe the probability of the capture process in binary interaction with an active site. Assuming an exponential dependence on R of the electron transfer interaction V that couples initial and final states, one obtains (Demkov 1964)

$$P^{site} = \frac{1}{2} \operatorname{sech}^2 \left(\frac{\pi}{2} \frac{\gamma \Delta E}{v} \right) \tag{11}$$

where γ characterizes the exponential decay of the electron transfer interaction $V = V_0 \exp(-\gamma R)$. The factor $1/2$ arises from the averaging over the trajectories with different impact parameters (Y). The parameter γ can be estimated from the decay length of the wave functions of the collisional partners: $\gamma^{-1} = \{\sqrt{2\varepsilon_{Hal^-}} + \sqrt{2\varepsilon_{A^-}}\}/2$.

The final probability of the negative ion formation can be then estimated from:

$$P^{total} = 1 - (1 - P^{site})^N \tag{12}$$

where N is the number of binary collisions. Note that the final negative ion formation probability can be large even for small P^{site}, provided the number of binary collisions N is large. The value of ΔE can be estimated from equation (8) and N can be estimated from the projectile trajectory. In fact, ΔE and N should be more looked at as adjustable parameters representing an effective energy difference and an effective number of collisions along the projectile trajectory. Despite their simplicity, equations (11) and (12) in conjunction with equation (8) have been successfully applied for the analysis of experimental data (Auth *et al* 1995a, 1998b, Auth 1996, Winter *et al* 1996b). In particular, they explain several experimentally observed features:

- the existence of the velocity threshold for the negative ion formation as due to the finite ΔE;
- the near threshold behaviour of the negative ion fractions as due to the velocity dependence of the binary capture probability (P^{site}) and cumulative effect (N);
- the shift of the negative ion formation threshold towards *larger* velocities for the same target surface with decreasing electron affinity of the projectile F(3.4 eV) $\rightarrow$ O(1.46 eV) $\rightarrow$ H(0.75 eV) as due to the ΔE decrease (see equation (8));
- the shift of the negative ion formation threshold towards smaller velocities for the same projectile, but changing the alkali halide target in order of increasing lattice constant: LiF ($a = 7.6\ a_0$) $\rightarrow$ KCl ($a = 11.9\ a_0$) $\rightarrow$ KI ($a = 13.3\ a_0$) (figure 5(b)) as due to the ΔE decrease with increasing a (see figure 8).

5.2.4. Parameter-free calculations of the F^- formation in grazing scattering at LiF(001), KI(001) and MgO(001) surfaces. Theoretical studies on F^- ion formation in grazing scattering at LiF(001), KI(001) and MgO(001) surfaces were performed by Borisov *et al* (1996), Borisov and Sidis (1997) and Deutscher *et al* (1999a). Later Deutscher *et al* (1999b) extended this study to the case of H^- formation in grazing scattering from MgO(001). Equation (10) was used to determine the total negative ion yield while the binary charge transfer probabilities $P(Y, Z)$, and, correspondingly, $P^{site}(Z)$ were obtained in the parameter-free study. In the case of the fluorine projectile equation (1) reads:

$$(\mathrm{AS})^{-q} + \mathrm{F}^0_{gas} \rightarrow (\mathrm{AS})^{-(q-1)} + \mathrm{F}^-_{gas} \tag{13}$$

where $(\mathrm{AS})^{-q}$ stands for the 'active site': (F^- for the LIF(001), I^- for the KI(001) and O^{-2} for the MgO(001) surface). F_{gas} is the projectile moving along the $\vec{R}(t) = (X = vt, Y, Z)$ trajectory, as sketched in figure 7. Owing to the open p-shell structure of the halide atom and O^- ion three substates emerge in the initial ($(\mathrm{AS})^{-q} + \mathrm{F}^0_{gas}$) and final ($(\mathrm{AS})^{-(q-1)} + \mathrm{F}^-_{gas}$) cases. These substates correspond to the permutations of the hole among three 2p-type orbitals of the fluorine projectile and np-type orbitals of the active site. The wave function of the interacting system is then expanded over a six-state basis :

$$\Psi = \sum_{k=1}^{6} a_k \phi_k \tag{14}$$

where the ϕ_k basis describe initial states where the hole is located at the $p_\mu(\mu = x, y \text{ or } z)$ orbital of the projectile and final states where the hole is located at the $p_\mu(\mu = x, y \text{ or } z)$ orbital of the active site. The orbitals are defined in the reference frame with the z axis along the *molecular* axis $\vec{R}$. This is the natural choice for a treatment of binary collisions. The other two axes are arbitrary and were chosen in such a way that the y axis lies in (or parallel to) the surface plane. The (x, y, z) reference frame can be obtained by an orthogonal rotation matrix from the fixed (X, Y, Z) reference frame attached to the surface.

The evolution of the wave function during the collision is given by the time-dependent Schrödinger equation. Assuming that the ϕ_k basis states in equation (14) are orthonormal, it takes the matrix form:

$$\mathrm{i}\frac{\mathrm{d}\boldsymbol{A}}{\mathrm{d}t} = (\mathbf{H} - \mathrm{i}\mathbf{T})\boldsymbol{A} \tag{15}$$

where $\boldsymbol{A}$ is the column vector of a_k coefficients in equation (14), $\mathbf{H}$ is the Hamiltonian matrix in the ϕ_k basis. $\mathbf{T}$ is a Coriolis coupling matrix that arises from the choice of the basis states in the rotating reference frame.

Hartree–Fock–Roothan self-consistent field (SCF) schemes were used to calculate the $\mathbf{H}$ matrix. In figure 9 we present the energy differences ΔE (differences between corresponding diagonal elements of the $\mathbf{H}$ matrix) and electron transfer interactions (off-diagonal elements of the $\mathbf{H}$ matrix) between p_z orbitals of the projectile and of the active site for the F/LiF and F/KI cases. p_z orbitals are oriented along the molecular axis and therefore experience the strongest electron transfer couplings. The results are presented along the trajectory parallel to the surface and passing over the active site: $\vec{R}(X) = (X, 0, Z = \text{const})$. Only positive values of the X coordinate are shown. As seen in the figure, the simple approach (equation (8)) gives a satisfactory estimate for ΔE. The differences from the SCF results arise from distortion of electronic clouds of the collision partners (polarization effects) which are present in the SCF calculation, but completely ignored in equation (8). In general, the results of SCF calculations confirm the predictions based on the simple model:

- the overall values of ΔE are much smaller for the F/KI(001) case compared to the F/LiF(001) case so that one would expect lower velocity thresholds and more efficient negative ion formation at the KI(001) surface;
- the energy differences ΔE increase with increasing atom–surface distance Z. This result together with a decrease of the charge transfer couplings with increasing Z predicts that the negative ion formation will be effective at small projectile–surface separations.

The distance dependence of the energy differences and electron transfer interactions obtained in the SCF study confirms the applicability of the Demkov–Nikitin model for the description of F^- formation on the LiF(001) surface. Similar features were found by Deutscher *et al* (1999a) for the F/MgO case. The situation is more complicated for F^- formation on the KI(001) surface. The ΔE difference might even go through zero in this case, as seen in figure 9(c). This feature indicates that, depending on the trajectory, a combination of the Landau–Zener curve crossing mechanism (Landau 1932, Zener 1932) and the Demkov–Nikitin near resonant mechanism (Nikitin 1962, Demkov 1964, Nikitin and Umanskii 1984) will concur in producing the F/KI(001) electron transfer.

Given the Hamiltonian matrix, equation (15) was integrated along the trajectory path parallel to the surface, and the probability of the negative ion formation by electron capture from the active site $P(Y, Z)$ and, correspondingly, $P^{site}(Z)$ were obtained. Realistic trajectories of the projectile were calculated on the basis of SCF derived pair interaction potentials, and equation (10) was used to obtain the final negative ion fractions. Comparison between experimental and theoretical results for F^- formation at LiF(001), KI(001) and MgO(001)

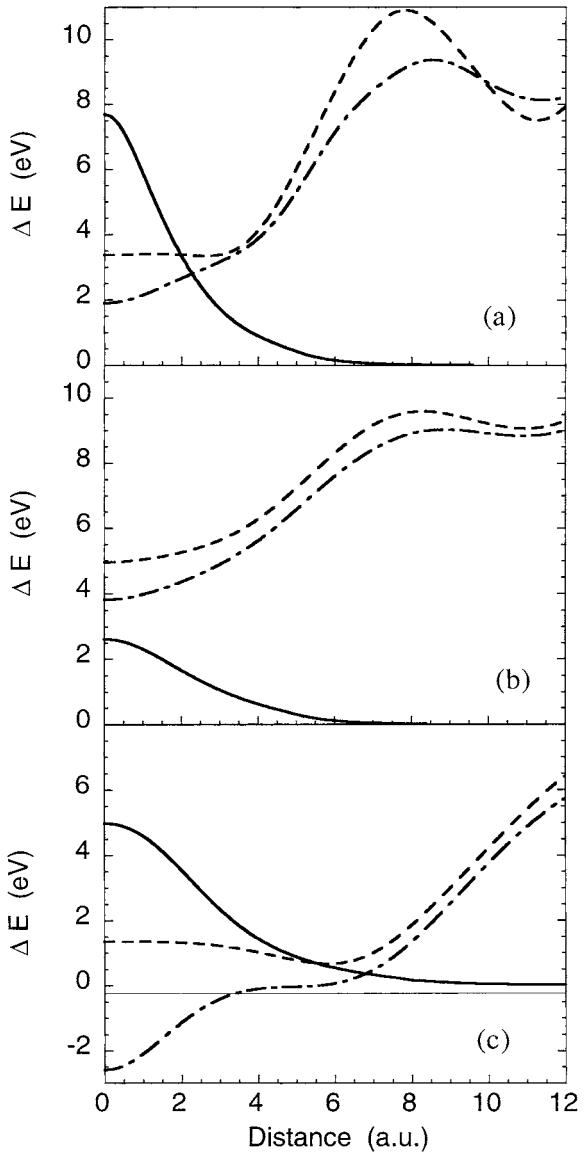

Figure 9. Diabatic energy differences (dashed–dotted lines) and electron transfer interactions (solid lines) from the parameter free calculations. Dashed lines represent energy differences obtained from the point charge approximation (equation (8)). Three situations corresponding to figure 8 are considered: (a) F/LiF(001) case, $Z = 2.5$ au; (b) F/LiF(001) case, $Z = 3.5$ au; (c) F/KI(001) case, $Z = 3.5$ au (Adapted from Borisov and Sidis 1997.)

surfaces is presented in figures 10 and 11. As seen in the figures the results of the parameter-free study reproduce quite well the low velocity part of the experimental data including the velocity thresholds for the negative ion formation. Note that the fast increase of the negative ion fraction after the threshold is not only due to the velocity dependence of the binary probability $P^{site}(Z)$ but also due to the increase of the number of binary collisions N with projectile velocity.

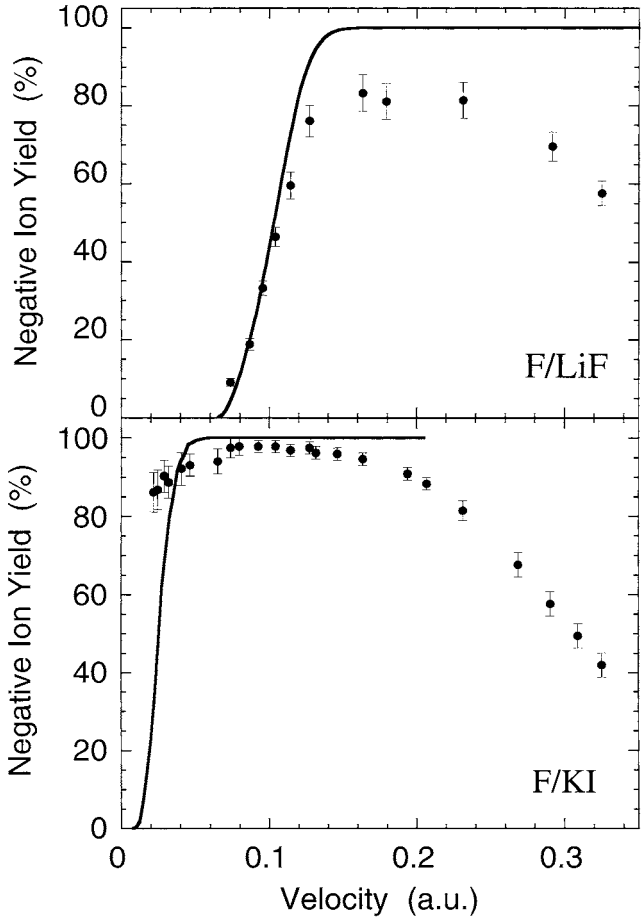

Figure 10. Comparison of measured and calculated negative ion yield, versus parallel velocity for Fluorine grazing scattering at LiF(001) and KI(001) surfaces. Dots with error bars represent experimental results, solid lines represent the theoretical results. The incidence angle of the scattered beam is 1° as measured from the surface plane. (Adapted from Borisov and Sidis, 1997.)

The theoretical results presented in figures 10 and 11 saturate for large velocities of the projectile, while the experimentally measured negative ion fractions decrease. The failure of the presented theoretical approach to reproduce the experimental data over the complete velocity range was attributed to the neglect of the electron loss process leading to the destruction of the negative ion (Auth *et al* 1995a, Winter *et al* 1996, Ustaze *et al* 1997b, Borisov and Sidis 1997, Deutscher *et al* 1999a, b). Unfortunately very little is still known about the electron loss process and quantitative information is available at the moment only for the H^-/LiF(001) system (see below).

5.2.5. Destruction of negative ions. Experiments on *negative ion beam* scattering at the MgO(001) surface by Ustaze *et al* (1997b) (see figure 4(d)) as well as recent energy loss measurements for hydrogen grazing scattering from the LiF(001) surface by Auth *et al* (1998a), Villette *et al* (1999) and Roncin *et al* (1999) clearly demonstrated the existence of the electron

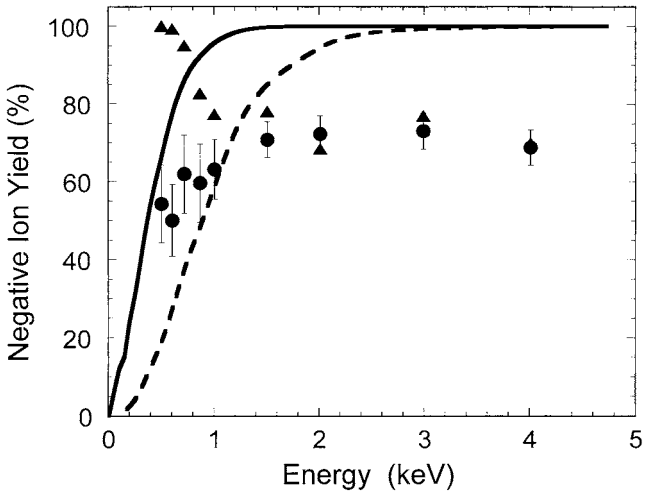

Figure 11. Total negative ion yield as function of the projectile energy for fluorine grazing scattering from MgO(001) surface. Symbols represent the experimental data by Ustaze *et al* (1997b). Dots: results obtained with impinging negative ions; triangles: results obtained with impinging neutral atoms. Lines represent results of the calculation with (solid line) and without (dashed line) inclusion of the polarization of the point charges lattice (Mott–Littleton interaction). (Adapted from Deutscher *et al* 1999a.)

loss channel. As already discussed, owing to the wide bandgap of the ionic crystals destruction of negative ions is generally suppressed. This is especially the case for the F^- ion with an affinity level lying inside the bandgap well below the bottom of the conduction band for all targets considered here (see figure 1(b)). That is why for incident F^- ions the negative ion reflection from the MgO(001) surface is complete at lowest energies (see figure 4(d)). In the same energy range the F^- fraction obtained with incident F atoms is much smaller, reflecting the existence of a velocity (energy) threshold for the negative ion formation. Increase of the projectile velocity results in the increase of the electron loss probability (the F^- fraction obtained with incident F^- ions decreases) and simultaneous increase of the electron capture probability (the F^- fraction obtained with incident F atoms increases). Finally, a dynamical equilibrium is reached when the outgoing negative ion fraction is independent of the charge state of the impinging projectile and is determined by the competition of the capture and loss rates. Compared to the F^- case, the electronic level of the O^- ion is situated much closer to the bottom of the conduction band of the MgO(001) surface and the vacuum level. One would expect that the destruction of negative ions is easier in this case. Indeed, at low energies the O^- fraction obtained with incident O^- ions is only slightly larger than that for the incident O atoms. Finally, for the loosely bound H^- ions, whose affinity level is in resonance with the conduction band, no 'memory' of the initial charge state is observed in the negative ion yield. This indicates that the electron loss probability is large enough in this case to quickly neutralize impinging negative ions and the situation becomes equivalent to that of an impinging neutral atom. One would expect that for e.g. the LiF(001) target the suppression of the electron loss channel would be more pronounced than for MgO(001) since the bottom of the conduction band is situated at +2.7 eV *above* the vacuum level (Lapiano-Smith *et al* 1991) (see also figure 1(b)).

The above features of the electron detachment explain why theoretical treatments neglecting electron losses were successful in giving a quantitative description of the

experimental data on F^- formation in the low energy (near formation threshold) region. This is because the electron losses are very small and the negative ion fraction is determined by the rapidly increasing electron capture probability. At the same time Deutscher *et al* (1999b) found that, even at low projectile energies, experimental data of Ustaze *et al* (1997b) on H^- formation in scattering from the MgO(001) surface can only be reproduced assuming a 98% electron loss probability per visited anion lattice site. Taking into account that for the LiF crystal electron losses should be less efficient, this finding is consistent with 40–50% electron loss probability per site deduced by Roncin *et al* (1999) from the H/LiF(001) energy loss data.

Different mechanisms of negative ion destruction were proposed to explain experimental findings although their relative efficiency is still an open question. These mechanisms are:

(1) promotion of the affinity level of the projectile into the continuum of conduction band or vacuum electronic states in the course of the short-ranged binary-type interactions with anion lattice sites at the surface (Ustaze *et al* 1997b, Esaulov *et al* 1999, Roncin *et al* 1999, Zeijlmans van Emmichoven *et al* 1999) leading to electron detachment;

(2) kinematically assisted electron transfer to the conduction band states (Winter *et al* 1996a, Lorente *et al* 1997, Ustaze *et al* 1997b). The underlying physics here is that the electronic states of the projectile and the surface are defined in the reference frames moving one with respect to the other. Translational factors (Bates and McCaroll 1958) should then be taken into account when discussing the relative energies of the affinity level and conduction band states. This modifies the target band structure in the projectile frame and might bring in resonance affinity level and conduction band states;

(3) electron detachment owing to the oscillating fields in front of the surface (Winter *et al* 1996a). Indeed, in the reference frame of the projectile alternating charges of the ionic crystal surface induce an oscillating field with a frequency proportional to the *velocity component parallel to the surface*. If the velocity is high enough, this oscillating field could induce transitions between electronic states of the projectile. This, so-called, resonant coherent excitation or Okorokov process (Okorokov 1965, Datz *et al* 1978, Kupfer *et al* 1981, Kimura *et al* 1996, Kimura and Mannami 1998, Garcia de Abajo and Echenique 1996, Hatke *et al* 1997) has been observed for the $1s \rightarrow 2p$ transition in atomic hydrogen grazingly scattered at an LiF(001) surface (Auth *et al* 1997, Winter *et al* 1999). In the same way oscillating fields might lead to electron loss by transitions from the bound states to the continuum states above the vacuum level (Garcia de Abajo *et al* 1992, 1994). Recent experimental findings confirm the existence of these coherent electron losses for the H^+ ion formation (Hecht and Winter 1998, Winter *et al* 1999) and destruction of H^- and F^- negative ions (Mertens and Auth 1998) in grazing scattering from the LiF(001) surface.

Recently the 3D wave packet propagation (WPP) approach was applied to study the electron detachment from H^- ions grazingly scattered from an LiF(001) surface (Borisov and Gauyacq 1999). The H^- ion has an open shell $1s1s'$ electronic structure with an inner tightly bound hydrogen-like 1s electron and an outer electron occupying a diffuse $1s'$ orbital and bound by only 0.75 eV. The electron loss process then concerns primarily the outer $1s'$ electron. The time-dependent Scrödinger equation for the wave function of the outer $1s'$ electron was then solved on the three-dimensional grid of points. An exact quantum mechanical treatment of the dynamics of the system together with different model representations of the LiF(001) surface allows us to assess the relative importance of different electron loss mechanisms discussed above. As a main result it was found that the electron detachment is driven primarily by the short-ranged interactions with the anion lattice sites. For slow collisions (600 eV—1 keV) and small projectile surface separations (2–3 au), owing to the

promotion of the H^- orbital into the continuum of vacuum states in front of the F^- sites at the surface, the electron detachment probability is extremely large (∼50%). This is in close agreement with the 40–60% value reported by Roncin *et al* (1999). The projectile has no time to probe the periodic potential of the crystal and coherent aspects of electron loss are difficult to observe. When the distance from the surface increases, the detachment probability per site decreases and the electron loss process reveals all the features of the resonant coherent detachment process, discussed by Garcia de Abajo *et al* (1992, 1994). In particular, the electron loss rate increases with increasing projectile velocity. As a further result of the WPP study it was found that electron emission proceeds primarily into the vacuum, electron loss into the conduction band states being much smaller. This is a result of the negative affinity of the LiF crystal with the bottom of the conduction band at +2.7 eV *above* the vacuum level (Lapiano-Smith *et al* 1991) so that the continuum of vacuum states is easier to reach. On the basis of the above results it was concluded that mechanisms (1) and (3) contribute mainly to the H^- destruction in front of the LiF(001) surface.

These results should be rather sensitive to specific projectile/surface combinations. Indeed, for the MgO crystal the bottom of the conduction band is below the vacuum level (Tjeng *et al* 1990, see figure 1(b)), so that one would expect that the relative efficiency of the electron losses towards the conduction band and vacuum states will change. Furthermore, the above discussion concerned only the outer 1s′ electron of H^-. At the same time, for small impact parameter fast collisions with surface atoms one would expect that the inner 1s electron can also be ejected despite its large binding energy. And indeed, formation of H^+ ions in grazing scattering of a hydrogen beam from the LiF surface was observed (Hecht and Winter 1998, Roncin *et al* 1999). Detachment of the inner electron would be an additional mechanism for the H^- destruction as this has been discussed also in gas-phase anion–atom collisions (see e.g. the review of Esaulov 1986).

To summarize, it is very likely that several (if not all) of the above mechanisms contribute to the destruction of the negative ions depending on the concrete projectile/surface combination. While the electron capture process leading to the negative ion formation seems to be understood, further work is needed to describe the negative ion destruction processes.

6. Concluding remarks

In conclusion we have thus seen that electron capture can occur very efficiently on semiconductors and on insulators. It has been suggested that in case of semiconductors an important role is played by surface states and that electron capture from such, rather localized, states could be described in a dynamic non-resonant charge transfer model. Quantitative descriptions have not been developed.

In the case of some oxides and alkali halides the capture process has a strongly localized character consistent with the ionic nature of these solids. In slow collisions capture has been discussed in terms of the adiabatic evolution of the molecular orbitals of small clusters. In fast collisions negative ion formation can be treated as a charge transfer process in the binary interaction between the projectile and the anion (oxygen or halide) surface site. The downward shift of the affinity level of the projectile due to the Madelung potential reduces the energy defect, making electron capture from the surface anion site possible. Once formed, a negative ion has a large probability to escape from the surface owing to the large bandgap of the ionic crystals that suppresses the electron loss channel. Existence of the loss channel was demonstrated by use of both atoms and negative ions as projectiles. Several mechanisms for the loss process have been proposed, but further work is needed to understand their relative

importance for different projectile/surface combinations. Both capture and loss channels must be properly taken into account to arrive at an accurate description of negative ion formation. These results also allow one to better understand the overall behaviour of negative ion formation on metal surfaces during their oxidation or chlorination from the submonolayer to the oxide/chloride film formation stage, when dielectric islands appear on the surface.

From a practical point of view these results show that scattering on ionic crystals could be efficiently used for production of negative ion beams, which is of much interest for hydrogen beam injection into plasma fusion devices: an application which in the past has been a major motive force in the studies of negative ion formation.

Acknowledgments

Many interesting discussions with C Auth, J P Gauyacq, C Henry, J Jupille, A Mertens, C Noguera, V Sidis, R Souda and H Winter are gratefully acknowledged. AGB. is indebted to C Auth, T Hecht, A Mertens and H Winter for frequent communication of the experimental data prior to publication. VAE acknowledges the stimulating collaboration of M Casagrande, O Grizzi, L Guillemot, J D O'Connor, S Lacombe, M Maazouz, S Ustaze and R Verucchi in many experiments described here.

References

Andryuschechkin B V, Eltsov K N, Shevlyuga V M and Yurov V Yu 1998 *Surf. Sci.* **407** L633
Auth C 1996 *PhD Thesis* Wechselwirkung von Atomen und Ionen mit Metall- und Isolatoroberflächen bei der Streifenden Streuung (Aahen: Sharker)
Auth C, Borisov A G and Winter H 1995a *Phys. Rev. Lett.* **75** 2292
Auth C, Hecht T, Igel T and Winter H 1995b *Phys. Rev. Lett.* **74** 5244
Auth C, Mertens A, Winter H and Borisov A G 1998a *Phys. Rev. Lett.* **81** 4831
Auth C, Mertens A, Winter H, Borisov A G and Garcia de Abajo F J 1997 *Phys. Rev. Lett.* **79** 4477
Auth C, Mertens A, Winter H, Borisov A G and Sidis V 1998b *Phys. Rev.* A **57** 351
Auth C, Winter H, Borisov A G, Bahrim B, Teillet-Billy D and Gauyacq J P 1998c *Phys. Rev.* B **57** 12 579
Bates D R and McCaroll R 1958 *Proc. R. Soc.* A **245** 175
Bahrim B, Borisov A G, Teillet-Billy D, Gauyacq J P, Wiegershaus F, Krischok S and Kempter V 1997 *Surf. Sci.* **380** 556
Behringer E R, Anderson D R, Cooper B H and Marston J B 1996 *Phys. Rev.* B **54** 14 765
Biswas R, Wang C Z, Chen C T, Ho K M and Soukoulis C M 1989 *Phys. Rev. Lett.* **63** 1491
Borisov A G and Gauyacq J P 1999 submitted
Borisov A G and Sidis V 1997 *Phys. Rev.* B **56** 10 628
Borisov A G, Sidis V and Winter H 1996 *Phys. Rev. Lett.* **77** 1893
Brako R and Newns D M 1989 *Rep. Prog. Phys.* **52** 655
Brudevoll T, Kotomin E A and Christensen N E 1996 *Phys. Rev.* B **53** 7731
Brongersma H H, Groenen P A C and Jacobs J-P 1994 *Science of Ceramic Interfaces* ed J Nowotny (Amsterdam: Elsevier) p 113
Burgdörfer J 1993 *Review of Fundamental Processes and Applications of Atoms and Ions* ed C D Lin (Singapore: World Scientific) p 517
Casagrande M, Lacombe S, Guillemot L and Esaulov V A 2000 *Surf. Sci.* **445** L29
Chen P J and Goodman D W 1994 *Surf. Sci.* **312** L767
Ciraci S, Butz R, Oellig E M and Wagner H 1984 *Phys. Rev.* B **30** 711
Colbourn E A 1992 *Surf. Sci. Rep.* **15** 281
Cornille J S, He J W and Goodman D W 1994 *Surf. Sci.* **306** 269
Coustet V and Jupille J 1994 *Surf. Sci.* **307–309** 1161
Datz S, Moak C D, Crawford O H, Krause H F, Ditter P F, Gomez del Campo J, Biggerstaff J A, Miller P D, Hvelplund P and Knudsen H 1978 *Phys. Rev. Lett.* **40** 843
Demkov Yu N 1964 *Sov Phys.–JETP* **18** 138

Deutscher S A, Borisov A G and Sidis V 1999a *Phys. Rev.* A **59** 4446
——1999b *Nucl. Instrum. Methods* B **157** 61
Dieckhoff S, Müller H, Maus-Friedrichs W, Brenten H and Kempter V 1992 *Surf. Sci.* **279** 233
Ducrée J J, Casali F and Thumm U 1998 *Phys. Rev.* A **57** 338
Esaulov V A 1986 *Ann. Phys. Paris* **11** 493
Esaulov V A, Guillemot L and Lacombe S 1999 *Comm. At. Mol. Phys.* **34** 273
Esaulov V A, Ustaze S, Maazouz M, Guillemot L and Verucchi R 1997 *Surf. Sci.* **380** L521
Fine J 1993 *Phys. Rev. Lett.* **71** 3585
Folkerts L, Schippers S, Zehner D M and Meyer F 1995 *Phys. Rev. Lett.* **74** 2204
Freund H-J 1997 *Angew. Chem.* **36** 453
Freund H J and Umbach E (eds) 1993 *Adsorption on Ordered Surfaces of Ionic Solids and Thin films (Springer Series in Surface Science 33)* (Heidelberg: Springer)
Fuggle J C 1977 *Surf. Sci.* **69** 581
García E A, Bolcatto P G, Passeggi M C G and Goldberg E C 1999 *Phys. Rev.* B **59** 13 370
Garcia de Abajo F J and Echenique P M 1992 *Phys. Rev.* **46** 2663
——1996 *Phys. Rev. Lett.* **76** 1856
Garcia de Abajo F J, Ponce V H and Echenique P M 1992 *Phys. Rev. Lett.* **69** 2364
——1994 *Phys. Rev.* B **49** 2832
Goniakowski J, Bouette-Russo S and Noguera C 1993 *Surf. Sci.* **284** 315
Grünert W, Schlögel R and Karge H G 1993 *J. Phys. Chem.* **97** 8638
Guseva M B, Babaev V G and Ubaidullaaev R R 1991 *Vacuum* **42** 613
Hägg L, Reinhold C O and Burgdörfer J 1997 *Phys. Rev.* A **55** 2097
Hatke N, Dirska M and Heiland W 1997 *Phys. Rev. Lett.* **79** 3395
Hayderer G, Schmid M, Varga P, Winter H P, Aumayr F, Wirtz L, Lemell C, Burgdörfer J, Hägg L and Reinholdt C O 1999 *Phys. Rev. Lett.* **83** 3948
Hecht T, Auth C, Borisov A G and Winter H 1996 *Phys. Lett.* A **220** 102
Hecht T and Winter H 1998 *Phys. Lett.* A **243** 306
Henrich V and Cox P A 1994 *The Surface Science of Metal Oxides* (Cambridge: Cambridge University Press)
Heiland W and Närmann A 1993 *J. Phys. C: Solid State Phys.* **5** A245
Hird B, Armstrong R A and Gauthier P 1993 *Surf. Sci.* **292** 305
Illas F, Lorda A, Rubio J, Torrance J B and Bagus P S 1993 *J. Chem. Phys.* **99** 389
Kasi K, Kang H, San C S and Rabalais J W 1989 *Surf. Sci. Rep.* **10** 1
Kempter V 1998 *Comments At. Mol. Phys.* **34** 11
Kimura K, Ida H, Fritz M and Mannami H 1996 *Phys. Rev. Lett.* **76** 3850
Kimura K and Mannami M 1998 *Phys. Rev.* A **57** 1121
King D A and Woodruf D P1988 *The Chemical Physics of Solid Surfaces and Heterogeneous Catalysis* (Amsterdam: Elsevier)
Kunz A B 1975 *Phys. Rev.* B **12** 5890
Kupfer E, Gabriel H and Bürgdorfer J 1981 *Z. Phys.* A **300** 35
Kurnaev V N, Koborov N N, Zhabrev G I and Zabeida O V 1993 *Nucl. Instrum. Methods Phys. Res.* B **78** 63
Landau L D 1932 *Phys. Z. Sow.* **2** 464
Lapiano-Smith D A, Eklund E A, Himpsel F J and Terminello L J 1991 *Appl. Phys. Lett.* **59** 2174
Ledyankin D V, Urazgildin I F and Yurasova V E 1988 *Sov. Phys.–JETP* **67** 2442
——1990 *Nucl. Instrum. Methods Phys. Res.* B **48** 585
Lorente N, Borisov A G, Teillet-Billy D and Gauyacq J P 1999 *Surf. Sci.* **429** 46
Lorente N, Merino J, Flores F and Gusev M Yu 1997 *Nucl. Instrum. Methods Phys. Res.* B **125** 277
Los J and Geerlings J J C 1990 *Phys. Rep.* **190** 133
Lowndes R and Martin D 1969 *Proc. R. Soc.* A **308** 473
Maazouz M, Baragiola R, Borisov A, Esaulov V A, Gauyacq J P, Guillemot L, Lacombe S and Teillet-Billy D 1996a *Surf. Sci.* **364** L568
Maazouz M, Borisov A G, Esaulov V A, Gauyacq J P, Guillemot L, Lacombe S and Teillet-Billy D 1996b *Phys. Rev.* B **55** 13 698
Maazouz M, Guillemot L, Lacombe S and Esaulov V A 1996c *Phys. Rev. Lett.* **77** 4265
Maazouz M, Guillemot L, Schlatholter T and Esaulov V A 1997 *Nucl. Instrum. Methods Phys. Res.* B **125** 283
Maazouz M, Ustaze S, Guillemot L and Esaulov V A 1998 *Surf. Sci.* **409** 189
Mahan G D 1980 *Phys. Rev.* B **21** 4791
Martin J S, Feranchak B T, Morris J R, Greeley J N and Jacobs D C 1996 *J. Phys. Chem.* **100** 1689
Martin J S, Greeley J N, Morris J R, Feranchak B T and Jacobs D C 1994 *J. Chem. Phys.* **100** 6791

Mertens A and Auth C 1998 private communication
Mertens A, Auth C and Winter H 1997 *Nucl. Instrum. Methods Phys. Res.* B **125** 293
Meyer F W, Yan Q, Ziejlmans van Emmichoven P, Hughes I G and Spierings G 1997 *Nucl. Instrum. Methods Phys. Res.* B **125** 138
Morris J R, Kim G, Barstis T L O, Mitra R, Quinteros C L and Jacobs D C 1997 *Nucl. Instrum. Methods Phys. Res.* B **125** 185
Morris J R, Martin J S, Greeley J N and Jacobs D C 1995 *Surf. Sci.* **330** 323
Mott N F and Littleton M J 1938 *Trans. Faraday Soc.* **34** 485
Müller H, Gador D, Wiegershaus F and Kempter V 1996 *J. Phys. B: At. Mol. Opt. Phys.* **29** 715
Müller H, Hausmann R, Brenten H and Kempter V 1994 *Surf. Sci.* **303** 56
Nikitin E E 1962 *Discuss. Faraday Soc.* **33** 14
Nikitin E E and Umanskii S Ya 1984 *Theory of Atomic Collisions (Springer Series in Chemical Physics, 30)* (Berliin: Springer)
Noguera C 1996 *Physics and Chemistry of Oxide Surfaces* (Cambridge: Cambridge University Press)
O'Connor D J and MacDonald R J. 1980 *Surf. Sci. Lett.* **100** L495
Okorokov V V 1965 *JETP Lett.* **2** 111
Olson R E 1972 *Phys. Rev.* A **6** 1822
Qian Guo-Xin and Chadi D J 1987 *Phys. Rev.* B **35** 1288
Rabalais J W (ed) 1994 *Low Energy Ion–Surface Interactions* (New York: Wiley)
Rechtein J H, Imke U, Snowdon K J, Reijnen P H F, Van den Hoek P J and Kleyn A W 1990 *Surf. Sci.* **227** 35
Renaud G, Villette B, Vilfan I and Bourret A 1994 *Phys. Rev. Lett.* **73** 1825
Roncin P, Villette J, Atanas J P and Khemlishe H 1999 *Phys. Rev. Lett.* **83** 864
Scheer J, Brüning K, Fröchlich T, Wurz P and Heiland W 1999 *Nucl. Instrum. Methods* B **157** 208
Scholze A, Schmidt W G and Bechstedt F 1996a *Phys. Rev.* B **53** 13 725
——1996b *Thin Solid Films* **281** 256
Shi M, Rabalais J W and Esaulov V A 1989 *Radiat. Effects and Defects in Solids* **109** 81
Somorjai G 1981 *Chemistry in Two Dimensions: Surfaces* (Ithaca, NY: Cornell University Press)
Souda R 1997 private communication
Souda R, Asari E, Kawanowa H, Suzuki T and Otani S 1999a *Surf. Sci.* **421** 89
Souda R, Hayami W, Aizawa T and Ishizawa Y 1993a *Surf. Sci.* **285** 265
Souda R, Hayami W, Aizawa T, Ohtani S and Ishizawa Y 1992 *Phys. Rev.* B **45** 14 538
——1993b *Phys. Rev.* B **47** 9917
Souda R, Suzuki T, Yamamoto K 1998 *Suf. Sci.* **397** 63
Souda R, Suzuki T, Kawanowa H and E Asari 1999b *J. Chem. Phys.* **110** 2226
Souda R and Yamamoto K 1997 *Nucl. Instrum. Methods* B **125** 256
Souda R, Yamamoto K, Hayami W, Tilley B, Aizawa T and Ishizawa Y 1995 *Surf. Sci.* **324** L349
Sousa C, Illas F, Bo C and Poblet J M 1993 *Chem. Phys. Lett.* **215** 97
Stracke P, Wiegershaus F, Krischok St, Müller H and Kempter V 1997 *Nucl. Instrum. Methods Phys. Res.* B **125** 63
Szymonski M 1990 *Desorption Induced by Electronic Transition / DIET IV (Springer Series in Surface Science 19)* ed G Betz and P Varga (Berlin: Springer) p 270
Tatewaki H and Miyoshi E 1995 *Surf. Sci.* **327** 129
Tjeng L H, Vos A R and Sawatzky G A 1990 *Surf. Sci.* **235** 269
Ustaze S, Guillemot L and Esaulov V A 1997a unpublished
Ustaze S, Verucchi R, Guillemot L and Esaulov V A 1997b *Phys. Rev. Lett.* **79** 3256
——1998 *Surf. Sci.* **397** 361
Ustaze S, Verucchi R, Guillemot L, Esaulov V A, Ochs R and Kempter V 1997c *Europhys. Lett.* **40** 329
van Wunnik J N M, Brako R, Makoshi K and Newns D M 1983 *Surf. Sci.* **261** 618
Varga P and Diebold U 1994 *Low Energy Ion–Surface Interactions* ed J W Rabalais (New York: Wiley) p 355
Verbeek H, Eckstein W and Bhattacharya R S 1980 *Surf. Sci.* **95** 380
Villette J, Atanas J P, Khemliche H, Barat M, Morozov V and Roncin Ph 1999 *Nucl. Instrum. Methods* B **157** 92
Wertheim G K, Rowe J E, Buchanan D N E and Citrin P H 1995 *Phys. Rev.* B **51** 13 675
Wiegershaus F, Krischok S, Ochs D, Maus-Friedrichs W and Kempter V 1996 *Surf. Sci.* **345** 91
Winter H 1991 *Comments At. Mol. Phys.* **26** 287
Winter H, Auth C and Borisov A G 1996a *Nucl. Instrum. Methods Phys. Res.* B **115** 133
Winter H, Auth C, Hecht T and Mertens A 1999 *Nucl. Instrum. Methods Phys. Res.* B **157** 32
Winter H, Mertens A, Auth C and Borisov A G 1996b *Phys. Rev.* A **54** 2486
——1997 *Phys. Rev.* A **55** R846
Wu J Z, Trickey S B, Sabin J R and Boettger J C 1995 *Phys. Rev.* B **51** 14 576

Wurz P and Becker C H 1989 *Surf. Sci. Lett.* **24** L559
Wurz P, Schletti R and Aellig M R 1997 *Surf. Sci.* **373** 56
Yu M L 1991 *Sputtering by Particle-Bombardement III (Topics in Applied Physics 64)* ed R Behrish and K Wittmaack (Berlin: Springer) p 91
Zeijlmans van Emmichoven P A, Niehaus A, Stracke P, Wiegershaus F, Krischok S, Kempter V, Arnau A, García de Abajo F J and Peñalba M 1999 *Phys. Rev.* B **59** 10 950
Zener C 1932 *Proc. R. Soc London* **137** 696
Zunger A and Freeman A J 1977 *Phys. Rev.* B **16** 2901
Zuo J M, O'Keefe M, Rez P and Spence J C H 1997 *Phys. Rev. Lett.* **78** 4777